Journal Pre-proofs

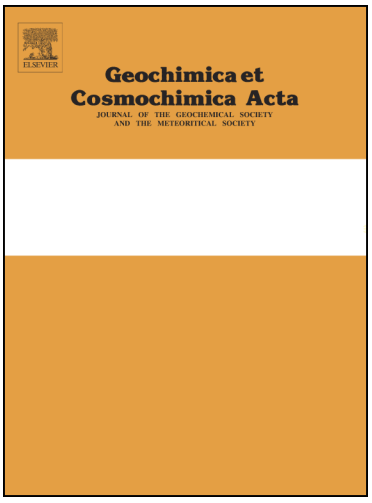

Uranium-series and strontium isotope systematics in soil carbonates from dryland Critical Zones: Implications for soil inorganic carbon storage and transformation

Syprose K. Nyachoti, Victor H. Garcia, Curtis Monger, Craig Tweedie, Thomas E. Gill, Lixin Jin, Lin Ma

PII: S0016-7037(24)00241-2
DOI: https://doi.org/10.1016/j.gca.2024.05.020
Reference: GCA 13426

To appear in: *Geochimica et Cosmochimica Acta*

Received Date: 31 October 2023
Accepted Date: 20 May 2024

Please cite this article as: Nyachoti, S.K., Garcia, V.H., Monger, C., Tweedie, C., Gill, T.E., Jin, L., Ma, L., Uranium-series and strontium isotope systematics in soil carbonates from dryland Critical Zones: Implications for soil inorganic carbon storage and transformation, *Geochimica et Cosmochimica Acta* (2024), doi: https://doi.org/10.1016/j.gca.2024.05.020

Uranium-series and strontium isotope systematics in soil carbonates from dryland Critical Zones: Implications for soil inorganic carbon storage and transformation

Syprose K. Nyachoti [1, †], Victor H. Garcia [1, §], Curtis Monger [2],

Craig Tweedie [3], Thomas E. Gill [1], Lixin Jin [1], and Lin Ma [1, *]

1. Department of Earth, Environmental, and Resource Sciences, University of Texas at El Paso, 500 W. University Ave., El Paso, TX 79902, United States
2. Department of Plant and Environmental Sciences, New Mexico State University, Las Cruces, New Mexico 88003, United States.
3. Department of Biological Sciences, University of Texas at El Paso, 500 W. University Ave., El Paso, TX 79902, United States.

† Current address: California Department of Toxic Substances Control, 700 Heinz Avenue, Suite 100, Berkeley, CA 94710, United States.

§ Current address: Arizona Geological Survey, 1955 East 6th Street, Tucson, AZ 85721, United States.

* Corresponding author: lma@utep.edu

Submitted to GCA in October 2023; Revised in May 2024

Key Words: Soil Carbonates, Critical Zone, U-series Isotopes, Sr Isotopes, Carbon Sequestration.

Abstract:

Soil carbonates are dominantly present in dryland Critical Zone (CZ) and their formation could lead to important long-term carbon sequestration in arid to semiarid soils if the Ca ions were derived from silicate weathering or other non-carbonate sources. In managed CZ systems such as agricultural areas converted from natural drylands, irrigation has profound effects on the dryland CZ inorganic carbon storage, especially by modifying dissolution and precipitation dynamics of soil carbonates via controls of irrigation intensity and water chemistry, soil properties, and hydrological flow paths. These processes could lead to transformation of inorganic carbon in soils and groundwater aquifers underneath drylands. One key knowledge gap in studying soil carbonates from managed dryland CZ systems is to detect the formation of soil carbonates under irrigated conditions and distinguish them effectively from soil carbonates formed under natural conditions.

Here, we explore the potential of using U-series and strontium isotopes to investigate the formation timescales and conditions of soil carbonates in both natural and managed dryland CZ in Chihuahua Desert of American Southwest. We obtained new U-series and Sr isotope ratios from mature stage V natural soil carbonates in the Jornada Basin of southern New Mexico and compared to previously published U-series and Sr isotope results for younger Jornada soil carbonates as well as irrigation impacted soil carbonates from the Rio Grande floodplains in west Texas. Specifically, we applied the U-

series dating method (^{238}U-^{234}U-^{230}Th) to estimate the timescales of soil carbonate formation under both natural climatic conditions and impacts of modern agriculture irrigation. In addition, we showed that the initial ($^{234}U/^{238}U$) activity ratios recorded in these soil carbonates reflect the systematic changes of soil infiltration rates in both natural and managed dryland CZ. We also utilized Sr isotope ratios ($^{87}Sr/^{86}Sr$) in soil carbonates, dust, and irrigation water to trace the Ca sources in soil carbonates from natural and managed dryland CZ. Soil carbonates from both settings were characterized by slightly radiogenic $^{87}Sr/^{86}Sr$ ratios, consistent with their potential of long-term carbon storage in drylands.

U-series and Sr isotope systematics characterize important differences in soil carbonates from natural and managed dryland CZ with respect to their Ca sources, timescales of carbonate formation and transformation, and availability of soil moisture. Soil carbonates formed, accumulated, and transformed in natural drylands with long time scales but under irrigated arid agricultural areas its formation is significantly modified by irrigation and other agriculture practices, with implications for long- and short-term inorganic carbon sequestration in both systems of drylands.

1. Introduction

The Earth's Critical Zone (CZ), a near-surface layer spanning from the vegetation canopy to the groundwater aquifer, is where rock, water, air, soil, and biota interact to support and sustain ecosystems and human lives (e.g., Brantley et al., 2006; Anderson et al., 2007; Brooks et al., 2015; Gaillardet et al., 2018). Extensive scientific networks of CZ observatories around the world have advanced a broader understanding of the CZ structure, function, and evolution, and integrated essential observational data into quantitative models to forecast CZ under impacts of anthropogenic and climatic changes (Brantley et al., 2006, 2011; Duffy et al., 2014; White et al., 2015; Rasmussen et al., 2015; Sullivan et al., 2016; Wymore et al., 2017; Gaillardet et al., 2018; Sullivan et al., 2019). Drylands, defined with an aridity index of 0.05-0.65 (annual rainfall over potential water loss via evapotranspiration; UNCCD, 2000), cover about 40% of the global land surface and provide habitat and resources for a global population of over two billion people (Grace et al., 2006; Wang et al., 2012). These fragile landscapes have essential roles and functions among the global CZ systems but have been facing increasing pressures and demands of water, food, energy, and land uses (Feng and Fu, 2013; Pravalie, 2016). The dryland CZ remains understudied despite of drylands' wide occurrences and unique characteristics at Earth's surface.

In the Chihuahua Desert of American Southwest (Fig. 1a), annual rainfall is low and episodic (mean precipitation < ~ 250 mm/year and most occurring in the summer monsoon season). Dryland soils are under long periods of low soil moistures but can experience flash wetting/flooding events during intensive monsoon storms (Noy-Meir, 1973; Reynolds et al., 2004; Newman et al., 2006; Nicholson, 2011; Duniway et al., 2018; Scott et al., 2019). One unique feature of the dryland soils is the accumulation of secondary carbonates, also known as pedogenic or soil carbonates (Fig. 1b and 1c) along with other evaporite minerals (such as opals, gypsum, and even halite; Zamanian et al., 2016). Global soil carbonates, with a dominant presence in drylands, contain about 700 to 940 Pg inorganic C ($1Pg = 10^{15}g$), which is the size of the atmospheric carbon pool and about two-thirds of the global soil organic carbon pool (e.g., Schlesinger et al., 1982; Eswaran et al., 2000; Monger and Martinez-Rios, 2001; Serna-Perez, 2006; Zamanian et al., 2016). Formation of soil carbonates in drylands has important implications of long-term carbon sequestration if the sources of Ca^{2+} are derived from silicate weathering or other non-carbonate sources. Furthermore, if dissolved inorganic carbon species from dissolution of soil carbonates move into groundwater aquifers underneath drylands, this process presents an important mechanism of short-term carbon storage (Monger et al., 2015). Indeed, soil carbonates and underlying groundwater aquifers in drylands have been recently recognized as one potential missing carbon sink in the global

carbonate budget, representing inorganic C fluxes as large as ~1 Pg C/yr (Houghton, 2007; Cole et al., 2007; Ma et al., 2014; Li et al., 2015).

Soil carbonates especially those in petrocalcic layers in drylands have low porosity and permeability, and greatly impact soil properties including soil texture, hydrological permeability, and partitioning coefficient between surface runoff and infiltration (Fig. 1c). Hence, soil carbonates are a key material in dryland CZ water and ecosystem research as they control the availability of soil moisture, infiltration rates, and unsaturated zone flows (e.g., Duniway et al., 2010; Zamanian et al., 2016). It is thus critical to investigate the formation and evolution of such a large inorganic carbon pool in natural dryland soils, to understand its complex control and feedback mechanisms with respect to the availability of soil moisture, and to predict its fate under future anthropogenic and climatic impacts on dryland systems.

In human managed dryland CZ such as agricultural areas converted from natural drylands, irrigation has produced profound effects on both organic and inorganic carbon pools. For example, intensive irrigation in worldwide arid and semi-arid areas has led to elevated soil salinity, sodicity, and alkalinity by loading dissolved solutes at accelerated rates from irrigation water (e.g., Sheta et al., 2000; Schoups et al., 2005; Jafari et al., 2012; Rath and Rousk, 2015; Cox et al., 2018). For example, irrigation with the Rio Grande water in far west Texas agriculture fields, typically with high dissolved Ca^{2+} and bicarbonate concentrations, has led to elevated rates of soil carbonates precipitation and release of abiotic CO_2 (Nyachoti et al., 2017; Cox et al., 2018; Ortiz et al., 2022). Carbon isotope systematics ($\delta^{13}C$) in soil carbonate, soil gas, and dissolved carbon species have identified significant contributions of abiotic CO_2 in soil gas in addition to biotic CO_2 in an irrigated pecan orchard in this region (Ortiz et al., 2022). Hence, irrigation has the potential to significantly modify or transform dryland land-atmosphere CO_2 flux and inorganic carbon storage. However, to date, such a potential shift in soil carbon dynamics associated with dryland agriculture is still poorly recognized and not included in models forecasting the future state of the Earth System. It is important to study soil carbonate dissolution/precipitation kinetics in managed dryland CZ systems to determine the potential impacts and its significance in local to biome-wide carbon cycling. One key knowledge gap is how to detect and quantify soil carbonate formation in managed dryland CZ and distinguish these soil carbonates effectively from those formed in natural drylands.

Here, we use uranium-series and strontium isotopes to investigate and distinguish the formation timescales and conditions of soil carbonates in natural vs. managed dryland CZ in Chihuahua Desert (Fig. 1). Natural dryland soils in the Jornada Basin in southern New Mexico, a typical alluvial basin in American Southwest (Fig. 2), contain significant amounts of pedogenic carbonates with various morphological stages (Gile et al., 1981). For example, natural soils of the La Mesa geomorphologic surface at the basin floor area contain mature soil carbonates as cemented and laminated horizons that were formed through the Quaternary period, and soils in piedmont slopes on the Jornada I geomorphologic surface contain relatively younger stage carbonates such as coatings and nodules (Fig. 2; Gile, 2002). In the Rio Grande alluvial valley and floodplains of southern New Mexico and west Texas (Fig. 2), the dryland CZ have been impacted by land use changes and agricultural practices such as crop production and irrigation for more than 100 years (Ortiz et al., 2022). We conducted a new U-series and Sr isotope study with the mature stage V soil carbonates on the La Mesa surfaces in the Jornada Basin and compared the results with the previously published U-series and Sr isotope datasets for younger Jornada I natural soil carbonates on the piedmont slopes in the Jornada Basin as well as irrigation impacted soil carbonates from the Rio Grande alluvial valley (Nyachoti et al., 2017; Ortiz et al., 2022). Our specific objectives are using soil carbonates in natural drylands and under the human managed conditions (irrigation) in agricultural areas: 1) to determine and compare the timescales of soil carbonate formation ; 2) to reconstruct the availability of soil moisture and soil infiltration rates with the initial ($^{234}U/^{238}U$) activity ratios recorded in soil carbonates, and 3) to use Sr isotope ratios to trace the sources of Ca in soil carbonates.

2. Background

2.1. Formation of soil carbonates in dryland CZ

It is well known that dissolved bicarbonate (HCO_3^-) ions react with calcium (Ca^{2+}) to form soil carbonates ($CaCO_3$), carbon dioxide (CO_2), and water (H_2O):

$$2HCO_3^- + Ca^{2+} \rightarrow CaCO_3(s) + CO_2(g) + H_2O \qquad \text{Eqn. 1.}$$

This reaction is driven by the saturation of Ca^{2+} and HCO_3^- in soil water under the impacts of topography, rainfall, temperature, soil texture and mineralogy, hydrology, and biology (Chadwick et al., 1999; Royer, 1999; Chiquet et al., 1999; Egli and Fitze, 2001; Hirmas et al., 2010; Laudicina et al., 2013; Gile et al., 1981; Eswaran et al., 2000; Tanner, 2010; Zamanian et al., 2016). Soil carbonates develop progressively with time into various morphological stages, including powders, filaments, coatings, nodules, cemented or laminated horizons (Fig. 1c) (Gile et al., 1981; Sobecki and Wilding 1983; Machette, 1985; Birkeland, 1999; Eswaran et al., 2000; Monger et al., 2006; Violette et al., 2010). The most mature and prominent soil carbonates (stage V) are petrocalcic layers with cemented and laminated horizons commonly observed in ancient and stable dryland landscapes, known locally as the "caliche" in American Southwest (e.g., Lahann, 1978; Chadwick et al., 1989; Royer, 1999; Chiquet et al., 1999; Egli and Fitze, 2001; Hirmas et al., 2010; Laudicina et al., 2013; Monger et al., 2015). The evolution of dryland CZ architecture is closely linked with different stages of soil carbonate developments.

2.2. U-series ages and initial $(^{234}U/^{238}U)_0$ ratios in soil carbonates

Uranium has three naturally occurring isotopes: ^{238}U (its half-life, $t_{1/2}$ = 4.46 Gyr), ^{235}U ($t_{1/2}$ = 700 Myr) and ^{234}U ($t_{1/2}$= 248 kyr) (Cheng et al., 2000). ^{234}U is produced through the alpha decay of ^{238}U. In old (>~1.3Ma) and unweathered rocks with a closed system, the activity of a daughter nucleus is equal to that of the parent and their activity ratio is equal to 1, e.g. $(^{234}U/^{238}U) = 1$. Such a system is in secular equilibrium (Bourdon et al., 2003). Here, activity refers to the product of the decay constant (λ) and the number of radio nuclei (N). During the associated alpha recoil process in water-rock interactions, ^{234}U is preferentially released compared to ^{238}U from rock weathering into water in two ways: (1) direct recoil of the short lived ^{234}Th, which later decays to ^{234}U, and (2) indirect release of ^{234}U from alpha recoil tracks (Fleischer, 1980). For this reason, natural waters such as soil water, stream water, groundwater, and ocean water are with characteristic $(^{234}U/^{238}U)$ activity ratios >1.

When soil carbonates precipitate, they inherit the high $(^{234}U/^{238}U)$ ratios > 1 from soil water. Over time, excess ^{234}U in soil carbonates decay to ^{230}Th, approaching the secular equilibrium value with time if soil carbonates remain as a closed system. The U-series systematics in soil carbonates enable calculating both ages and the initial $(^{234}U/^{238}U)$ ratios hereafter abbreviated as $(^{234}U/^{238}U)_0$ in soil water at the time of the soil carbonate formation. However, soil carbonates usually contain U and Th from detrital silicate fractions (Bischoff and Fitzpatrick, 1991; Edwards et al., 2003; Neymark, 2011). Isochron techniques are commonly employed to get detrital free carbonate end-member $(^{230}Th/^{238}U)$ and $(^{234}U/^{238}U)$ activity ratios in soil carbonates (Ludwig, 2003; Paces et al., 2012). Techniques such as weak acid leachate/residue, leachate/leachate, or total sample dissolution methods have been applied on bulk soil carbonates to obtain a set of cogenetic samples that formed around the same time with different portions of detrital components (Bischoff and Fitzpatrick, 1991; Edwards et al., 2003; Neymark, 2011). $(^{230}Th/^{232}Th)$, $(^{238}U/^{232}Th)$, and $(^{234}U/^{238}U)$ ratios in cogenetic samples are used to construct 2D or 3D isochrons with geochronology software Isoplot® (Osmond et al., 1970; Rosholt, 1976; Ludwig, 2003). It is important to note that such correction techniques are operational and assume: 1) the pure carbonates precipitating from soil water contain no Th due to its low solubility; 2) there are only two isotopically homogeneous end members in soil carbonates: detrital materials vs. authigenic carbonates; and 3) the system remains closed after formation of carbonates (Bischoff and Fitzpatrick, 1991; Luo and Ku, 1991).

In addition to formation ages, the initial ($^{234}U/^{238}U$) ratios recorded by soil carbonates are a hydrologic indicator of rainfall amounts or soil water infiltration rates (Robinson et al., 2004; Oster et al., 2012; Maher et al., 2014). The degree of ($^{234}U/^{238}U$) disequilibrium in soil water, streams, and rivers is controlled by the alpha recoil process under the impact of climatic parameters such as mean annual rainfall that controls the balance between chemical weathering vs. physical erosion (Chabaux et al., 2003; 2008; Maher et al., 2004; 2006; DePaolo et al., 2006; Robinson et al., 2004; Andersen et al., 2009; Strandmann et al., 2010; Oster et al., 2012). Indeed, ($^{234}U/^{238}U$) ratios in soil water hypothetically decrease with the increasing chemical dissolution rates and the increasing water availability for rock weathering to occur (infiltration, runoff, and rainfall). Therefore, high rainfall results into low ($^{234}U/^{238}U$) ratios in soil waters due to complete rock dissolution, thus reduced selective loss of ^{234}U and low rainfall, on the other hand, leads to high ($^{234}U/^{238}U$) ratios in soil waters due to preferential release of ^{234}U into weathering fluids by enhanced alpha recoils. The dependence of ($^{234}U/^{238}U$) ratios in soil water on rainfall amounts in a watershed has shown the great potential of using ($^{234}U/^{238}U$) ratios recorded in secondary soil minerals such as soil carbonates and opals to quantify soil water infiltration rates and soil moisture availability (Oster et al., 2012; 2017; Maher et al., 2014; McGee et al., 2012).

2.3. $^{87}Sr/^{86}Sr$ isotope ratios to trace calcium sources in soil carbonates

Strontium isotope ratios ($^{87}Sr/^{86}Sr$) in soil carbonates of arid and semiarid areas have been widely used as a tracer for identifying the Ca sources, especially distinguishing their origins from carbonate vs. silicate materials (Capo et al., 1998; Capo and Chadwick, 1999; Chiquet et al., 1999; Naiman et al., 2000; Van Der Hoven and Quade, 2002). Many bedrock types develop different $^{87}Sr/^{86}Sr$ ratios because their Rb/Sr ratios and bedrock ages control radiogenic ^{87}Sr ingrowth from decay of ^{87}Rb (e.g., Bullen et al., 1996). Typically, silicate-derived Sr has higher $^{87}Sr/^{86}Sr$ ratios than carbonate-derived Sr. Indeed, dissolved $^{87}Sr/^{86}Sr$ ratios of ~30 global rivers compiled by Tripathy et al. (2010) range widely from 0.709 to 0.729, controlled by the mixing proportion of Sr contributed by carbonates (~0.707-0.708) vs. silicates (e.g., >0.720) in their watersheds. In addition, GIS-based models were built to map Sr isotope ratios in rocks and waters with combined effects of lithology and bedrock ages at regional scales across the contiguous USA (Bataille and Bowen, 2012). Such lithology modelling works provide an important framework and baseline to constrain the $^{87}Sr/^{86}Sr$ ratios in soil carbonates for regional studies.

3. Methods

3.1. Study areas

3.1.1. Natural drylands in Jornada Basin: Basin floor and piedmont slope sites

The Jornada Basin is an intermontane basin in the Basin and Range province in American Southwest (Figs.1 and 2). The Jornada Basin is part of the Chihuahuan Desert ecosystem with semi-arid to arid climates. Its annual precipitation is ~ 210-250 mm/year and most occurring during the summer monsoon season (National Climatic Data Center). Annual potential evapotranspiration at the Jornada Basin is very high at ~2200 mm/year and mean annual air temperature is ~16 °C (Gile et al., 1981). Vegetation in the Chihuahuan Desert has gradually transformed from grassland to shrubland plant communities probably due to climate changes during the past ~20,000 years and land use changes in recent 100 years (Van Devender, 1995; Monger, 2003; Snyder and Tartowski, 2006; Weems and Monger, 2012). Current plant communities include five major vegetation types: mesquite (*Prosopis glandulosa*), tarbush (*Flourensia cernua)*, black grama grass (*Bouteloua eriopoda*), creosotebush (*Larrea tridentata*), and playa grasslands (Gibbens et al., 2005; Bergametti and Gillette, 2010).

The Jornada basin is bounded to the east by north-south trending block faulted San Andres and Organ mountains and to the west by Dona Ana and Caballo Mountains (Fig. 2) (Seager et al., 1984; Mack

et al., 1998; Hawley, 1981). Typical bedrocks on the mountains and hills areas (Fig. 2) include Paleozoic sedimentary rocks, mainly fossiliferous limestone, sandstone, and shale, and Precambrian metamorphic rocks intruded by Tertiary volcanic and plutonic rocks (Mack et al., 1998; Monger et al., 2006). Exposed bedrocks on the mountain flanks were eroded and moved downslope filling the piedmont slopes (bajadas or Jornada I) and basin floor (La Mesa surface) over time (Fig. 2; Mack et al., 1993).

The La Mesa geomorphic surface is the oldest surface with late Pliocene to middle Pleistocene ages (Gile et al., 1981; Gile, 2002). The soils of the La Mesa surface are developed on alluvium deposits overlying fluvial sediments (Camp Rice Formation) that were deposited between 5 Ma and 0.8 Ma when the ancestral Rio Grande ran through the Jornada Basin (Gile et al., 1981; Mack et al., 2012). The parent Camp Rice Formation sediments contain minimal carbonates (<1% $CaCO_3$) (Gile et al., 1981; Capo and Chadwick, 1999). The soils commonly contain stage V soil carbonates and are estimated to be about 1.6 Ma in age (Mack et al., 1993; 1996).

The relatively young Jornada I geomorphic surface (approximately 500 ka to 700 ka) is located on the piedmont slopes of mountain ranges (Fig. 2; Serna-Perez et al., 2006; Monger et al., 2009). These younger sediments include a mixture of clay, silt, sand, and pebbles and form the parent material of soils on the piedmont slopes (Seager et al., 1984). The soils on the Jornada I geomorphic surface contain soil carbonates with stage I-II development as well as old petrocalcic horizons ("caliche") with stage IV and V development (Gile et al., 1981).

The Jornada Basin and its surrounding drylands have been considered as a significant North American dust source area (Monger, 2006; Rivera et al., 2010). Various dust sources are located at basin floor, playas, bare (unvegetated) soil surface, and agricultural fields within the Chihuahua desert, depending on soil moisture, wind speed, threshold wind velocity, and type of land surface (Gillete, 1999; Gillette and Chen, 2001; Rivera et al., 2010; Klose et al., 2019). Geomorphic surfaces are generally wind-eroded with deflation and depositional features oriented in the prevailing west-southwest wind direction (Monger et al., 2006).

3.1.2. Managed drylands in Rio Grande valley: agricultural sites in West Texas

Agricultural fields are commonly distributed along the Rio Grande valley in west Texas and southern New Mexico (Fig. 2). Agricultural soils in these human managed dryland areas are developed on alluvium deposits of the Rio Grande valley and are classified as Entisols and Aridisols (Miyamoto and Chacon 2006). These floodplains belong to the Holocene Fillmore geomorphic surface (100 yrs to 7000 yrs B.P).

Soil carbonates were studied in two representative agricultural sites in El Paso County, Texas: 1) a pecan orchard in Tornillo, TX and 2) an alfalfa field in El Paso, TX (Cox et al., 2018; Nyachoti et al., 2017; Ortiz et al., 2022). The pecan site has been cultivated for approximately 40 years, and prior for cotton for 60 years. The alfalfa site has only been cultivated for alfalfa. These agricultural fields are flood irrigated, primarily with Rio Grande water. The pecan orchard is typically irrigated from April to October during the growing season, once every two to three weeks with approximately 10 to 12 irrigation events or on average ~1.2 m of water annually. When river water is insufficient, the pecan orchard would be irrigated using local groundwaters, while the alfalfa field is left fallow. In addition, the pecan orchard is fertilized and amended by sulfur and gypsum pellets to lower soil sodicity. The alfalfa site is less managed and has no history of soil amendments or fertilization.

3.2. Soil and dust sample collection

Soil carbonates of the Jornada Basin were collected from one excavated trench profile (15 m wide and 2.5 m deep; Latitude 32.600978°; Longitude -106.830411°) at the La Mesa surface on the Basin floor site (Fig. 2). The trench exposes a thick and well-developed (cemented and laminated) soil carbonate horizon with stage V development (Fig. 3a). The horizon is thickest at the center (~2 m; Fig. 3d), decreases in thickness to the sides suggesting possible surficial disturbance by erosion, sedimentation, or rooting/bioturbation. The soil carbonate horizon is also extensively fractured and has an abrupt upper boundary with the topsoil, which consists of ~40 cm thick unconsolidated sandy materials with stage I carbonates. The sharp boundary is characterized by brittle to massively calcified, smooth micritic carbonate laminae (Robinson et al., 2015). In some areas, morphology of the soil carbonate horizon is botryoidal suggesting possible growth into open space or more likely are evidence of dissolution pipes that have been partially infilled by round concretionary masses (pisoids) that cemented together by overlapping carbonate laminae (Robinson et al., 2015). On vertical profiles inside the trench, multiple soil carbonate samples at various depths from ground surface were collected for analysis in this study (Table 1).

At the Jornada Piedmont slopes, soil carbonates with stage I-II developments were previously collected from two 50-cm deep soil pits (JPT1 and JPT2; e.g., Fig. 3b) at approximately 5 m apart (Latitude 32.582812°, Longitude -106.634589°; Nyachoti et al. 2017). Soil samples were collected at 5 cm interval from land surface to the upper boundary of the caliche layer at each pit (40 and 48 cm at JPT1 and JPT2, respectively). In addition, two caliche samples were collected from the bottom of the two soil pits with cemented horizons (from 40 cm depth at JPT1 and 48 cm depth at JPT2; Fig. 3e). The caliche layers are consisted of large gravels (~5 to 10 cm size) with ~ 1 cm-thick carbonate coatings.

Agricultural soil samples with very early stages of soil carbonate developments were collected from soil pits and auger holes at the Alfalfa (Latitude 31.067103°; Longitude -106.262339°; Fig. 3c) and Pecan sites (Latitude 31.404153°; Longitude -106.054150°) previously described by Cox (2012), Cox et al. (2018), Nyachoti et al. (2019) and Ortiz et al. (2022). Briefly, soil samples were collected at 10 cm intervals from the wall of the pit until depth or collected at 10 cm intervals from auger holes until depth of refusal.

Modern dust samples, previously collected from the Jornada Basin between 2005 and 2006 by Bergametti and Gillette (2010), were included in this study. Briefly, dust samples were collected with Big Spring Number Eight (BSNE) dust samplers at 5, 10, 20, 50, and 100 cm above ground at various sites at the Jornada Basin. Sample sites were chosen based on the dominant vegetation and the need to assess the effect of vegetation on dust mass fluxes.

Bulk soil samples were air-dried and pulverized to pass through 100μm sieve. Caliche samples were saw-cut and then drilled along different laminar layers. The layers are thought to have formed from infiltrating soil waters which are impaired from draining down the soil profile due to underlying plugged horizons (Gile et al., 1981). In general, when possible three layers in each caliche hand sample were sampled and labeled as A, B, and C, where A is bottommost while C is the upper or outermost laminae.

3.3. U-series isotope analysis

In order to generate a set of cogenetic samples for U-series isochron analysis, soil carbonate samples were split and subjected to varying chemical treatments including total sample digestion (TSD) and acid-leachate techniques (L/R). For the acid-leachate techniques, three portions of ~100 mg of the soils and carbonate samples were used. The first aliquot of soil and soil carbonate were digested as bulk total digestion samples with strong acids (HNO_3 and HF followed by HCl and H_3BO_3). The second and third aliquots of soil and carbonate samples were leached with 10ml 1N HCl and 10 ml 1N acetate acid (AcOH) respectively for 30 minutes. After leaching, the HCl leachate (HCl-L) and the acetic acid leachate (AcOH-L) were separated from residues (HCl-R and AcOH-R) by centrifuging and decanting and digested with

strong acids. A selected number of samples were only processed with the 1N AcOH acid leaching procedure. All the samples were digested along with a combined ^{233}U-^{229}Th spike for U and Th isotope dilution analysis.

Analytical procedures for U and Th concentrations and isotopic compositions are from Pelt et al. (2008). Column chemistry procedures were conducted for separation and purification of U and Th through AG 1-X8 anion exchange resin (200-400 mesh) in a class-100 cleanroom at University of Texas at El Paso (UTEP). The purified U and Th samples were measured for the following isotopic ratios using the standard-sample bracketing method on a Nu Plasma High Resolution Multi Collector Inductively Coupled Plasma Mass Spectrometry (MC-ICP-MS): $^{234}U/^{238}U$, $^{233}U/^{238}U$, $^{235}U/^{238}U$, $^{230}Th/^{232}Th$, and $^{229}Th/^{232}Th$. Uranium and Th concentrations were calculated by the isotope dilution method. Uranium and Th activity ratios were calculated from ion count gain and mass fractionation corrected isotope ratios as well as the half-lives after Cheng et al. (2000). A reference rock material (USGS BCR2) was regularly measured to assess for accuracy with average U concentrations of 1.689 ± 0.018 ppm (n = 25, 2σ) and Th concentrations of 5.86 ± 0.07 ppm (n = 10, 2σ). Measured ($^{234}U/^{238}U$) of the BCR2 were at equilibrium values with averages of 1.002 ± 0.005 (n = 25, 2σ) and average ($^{230}Th/^{232}Th$) ratios a 4.895 ± 0.011x 10^{-6} (n = 10, 2σ). All these ratios were within the errors reported from other laboratories (Sims et al., 2008). Procedure blanks were negligible (~4 pg U and ~100 pg Th).

3.4. Sr isotope analysis

Strontium isotope analyses ($^{87}Sr/^{86}Sr$ ratios) were conducted on soils, soil carbonates, and dust samples from the basin floor site in this study following procedures in Konter and Storm (2014). Approximately 50 mg of dust and 100 mg of powdered soil and caliche samples were weighed in two portions. One portion (the bulk) was totally digested in HF and HNO_3 followed by HCl and boric acid digestion. The second portion was leached with ~10ml 1N acetic acid for 30 minutes. Residues were separated from the supernatant and acid-digested in two steps while the leachates were evaporated to dryness. The digested bulk, residues and leachate samples were re-dissolved in 3.5N HNO_3 and passed through Sr-Spec resin to separate Sr from the matrix. The purified samples were then analyzed for $^{87}Sr/^{86}Sr$ isotopes on the MC-ICPMS using standard-sample bracketing method, with the Sr isotope standard SRM 987 as the bracketing solution (average $^{87}Sr/^{86}Sr$ ratio = 0.71024 ± 0.00001; 2SD, n=32). For quality control purposes, BCR2 rock standards were treated as bulk samples with measured average $^{87}Sr/^{86}Sr$ ratio of 0.70502±0.00001 (2SD, n=9), which were within the values reported in literature (Jochum et al., 2016). Procedure blanks were negligible (~80 pg Sr).

4. Results

In this study, U-series activity ratios ($^{234}U/^{238}U$ and $^{230}Th/^{238}U$), U and Th concentrations, and Sr isotope ratios ($^{87}Sr/^{86}Sr$) ratios were reported for the soil carbonate samples of the basin floor site (BF-series) on the La Mesa surface of the Jornada Basin (Table 1 and 2). Soil carbonate samples from the piedmont slope sites (PD-series) on the Jornada I surface and the agricultural fields (AG-series) from the Rio Grande valley floodplains (Nyachoti et al., 2019; Ortiz et al., 2022) were listed in Table 3 for comparison.

4.1. ($^{234}U/^{238}U$) and ($^{230}Th/^{238}U$) ratios in natural dryland soil carbonates

In the La Mesa trench profile, soil carbonates from shallow depth (0-40 cm) are mainly in the forms of powders and small nodules while the underlying soils at 40-250 cm depth are consisted of thick petrocalcic layers of clast coatings, cemented clasts, and laminated horizons (Fig. 3d). It is difficult to physically separate pure carbonates from the bulk matrix. As described in the method section, weak acid

leaching procedures (with 1M acetic acid or 1M hydrochloric acid) were operationally applied to obtain carbonate elemental and isotopic compositions (Bischoff and Fitzpatrick, 1991; Edwards et al., 2003; Maher et al., 2006; Neymark, 2011).

($^{234}U/^{238}U$) ratios of bulk soil carbonate samples (BF-1 to BF-9) range from 0.91 to 1.37, with most values greater than 1.0 and indicating the dominant presence of carbonates in these soils that precipitated from soil water with ($^{234}U/^{238}U$) ratios >1 (Fig. 4a; Table 1). Indeed, ($^{234}U/^{238}U$) ratios of their weak acid leachate samples, representing the carbonate signatures of these samples, are all higher than their respective bulk samples (Fig. 4a). By contrast, the silicate-rich leaching residual samples are characterized with lower ($^{234}U/^{238}U$) ratios (Fig. 4a).

($^{230}Th/^{238}U$) ratios of these soil carbonates are expected to show complementary trends to those of the ($^{234}U/^{238}U$) ratios, i.e. with values decreasing from the residual, to bulk, and to weak acid leachate samples. Most samples show the expected trend except for the soil carbonate samples BF-1, BF-3A, BF-7, and BF-9 that show higher ($^{230}Th/^{238}U$) ratios in weak acid leachate samples (Table 1). The presence of these unusually higher ($^{230}Th/^{238}U$) ratios in those samples could be due to laboratory artifacts during the leaching experiments by either excessive leaching of ^{230}Th from silicate minerals or possible re-adsorption of U from leachates back to residual materials (Menozzi et al., 2016). Hence, this specific subgroup of soil carbonate samples (BF-1, -3A, -7, -9) may not obtain U-series isochrons (see section below).

4.2. U-series isochron model ages and initial ($^{234}U/^{238}U)_0$ ratios

The activity ratios of ($^{234}U/^{238}U)_t$ and ($^{230}Th/^{238}U)_t$ of a pure carbonate sample evolve as a function of time t and initial ratio ($^{234}U/^{238}U)_0$:

$$\left(\frac{^{234}U}{^{238}U}\right)_t = \left(\frac{^{234}U}{^{238}U}\right)_0 e^{-\lambda_{234}t} + (1 - e^{-\lambda_{234}t}) \quad \text{Eqn. 2,}$$

$$\left(\frac{^{230}Th}{^{238}U}\right)_t = \left(\frac{\lambda_{230}}{\lambda_{230}-\lambda_{234}}\right)\left(\frac{^{234}U}{^{238}U}\right)_0 (e^{-\lambda_{234}t} - e^{-\lambda_{230}t}) + \left(1 + \frac{\lambda_{234}e^{-\lambda_{230}t} - \lambda_{230}e^{-\lambda_{234}t}}{\lambda_{230}-\lambda_{234}}\right) \quad \text{Eqn. 3,}$$

here, λ_{234} and λ_{230} are the decay constants for ^{234}U and ^{230}Th, respectively. The majority of the U-series ratios of the weak acid leachates from the basin floor site are compared to their respective positions on the classic U-series isotope evolution diagram (Fig. 4b), consistent with age spans from ~10 kyrs to >400 kyrs and initial ($^{234}U/^{238}U$) ratios ranging from 1.1 to 1.6. For comparison, weak acid leachates of soil carbonates from the Piedmont slopes of the Jornada Basin (Nyachoti et al., 2017) showed age spans of ~ 100 kyrs to 300 kyrs and initial ($^{234}U/^{238}U$) ratios of ~1.2-1.7. Soil carbonates from the agricultural fields (Nyachoti et al., 2017) show age spans significantly younger than 100 kyrs and distinctively lower ($^{234}U/^{238}U)_0$ ratios (~1.2-1.4) (Fig. 4b). However, it is evident that several soil carbonates with high ($^{230}Th/^{238}U$) ratios in their weak acid leachates (e.g., BF-1, -3A, -7, -9; Fig. 4b) plot outside of the general range of U-series isotope evolution curves.last section. It is clearly that these four samples do not follow any reasonable U-series isotope evolution curves.

U-series ages and initial ($^{234}U/^{238}U)_0$ ratios of 13 sets of soil carbonates from the basin floor trench profile were calculated with the program ISOPLOT R (Table 3; Ludwig, 2003; Vermeesch, 2018). The sets of cogenetic samples were generally obtained from using several sub-samples for total sample digestion (TSD method) or combining acid leachate/residual samples (L-R method) (Luo and Ku, 1991). We used both TSD and L-R methods with the Rosholt Maximum likelihood model and the number of data points for each isochron ranges from 3 to 8. Individual U-series isochrons for all sets of cogenetic samples are provided in Appendix Figures and the model fitting parameters are listed in Table 3. Among the 13 sample sets, 8 sample sets (BF-2A, -2B, -2C, -3C, -4B, -4C, -6, and -8) have U-series ages and

initial $(^{234}U/^{238}U)_0$ ratios with model fitting parameters ranging from generally reasonable to poorly fitted values, as indicated by their mean square of weighted deviates (MSWD = 0.9 to 110) and probability of fit (p chi^2 = 0 to 0.42; Table 3). It is noted that three sample sets (BF-1, -7, and -9), all with unusually high ($^{230}Th/^{238}U$) ratios as mentioned above, do not yield any U-series isochrons and two sample sets (BF-3A and -4B) only yield ages with very large error bars (Table 3).

The presence of poor model fits highlights the general difficulty of U-series dating in soil carbonates: the observed scatter of the data about the isochron cannot be quantitively compared with the assigned analytical errors, indicating the presence of scatter related to the fundamental assumptions of an isochron including 1) the samples formed at the same time, 2) their parent and daughter isotopes were initially homogeneous, and 3) they behaved as a closed system. Hence, it is likely that the soil samples could contain a mixture of carbonates with different formation ages, multiple detrital components, or not in a closed system since formation. Here, we acknowledge such challenges and do not intend to use the age models to precisely date carbonates. Instead, we focus on comparing information derived on soil carbonates from broadly different formation ages within the uncertainties. Despite the challenges and uncertainties of the age dating involved in soil carbonates, numerous studies have shown that soil carbonates, due to their wide occurrence in soil zones around the world and their abilities of recording various environmental conditions, provided invaluable information for Earth surface processes, especially related to water fluxes and soil conditions. Indeed, in this study soil carbonates from the trend profile with ages younger than 20 kyrs have relatively higher $(^{234}U/^{238}U)_0$ ratios (1.5-1.7) than soil carbonates from 20 -100 kyrs with $(^{234}U/^{238}U)_0$ ratios (1.1 -1.5), despite of the large uncertainties.

4.3. $^{87}Sr/^{86}Sr$ ratios in soil carbonates and dusts

Sr isotopic ratios ($^{87}Sr/^{86}Sr$) in the carbonate and silicate portions of soil carbonates were obtained for the basin floor La Mesa trend profile and for the dust samples around the Jornada Basin (Fig. 5). The carbonate portions in soil carbonates from the basin floor trend profile have $^{87}Sr/^{86}Sr$ ratios ranging from 0.7086 to 0.7123, while their corresponding silicate portions have a much higher and broader range of $^{87}Sr/^{86}Sr$ ratios from 0.7098 to 0.7250. For modern dust samples collected around the Jornada Basin, the carbonate portions show a narrow range of $^{87}Sr/^{86}Sr$ ratios from 0.7087 to 0.7091 while the silicate portions have much higher $^{87}Sr/^{86}Sr$ ratios with a wide range from 0.7119 to 0.7225. The $^{87}Sr/^{86}Sr$ ratios in dust carbonates from Jornada Basin are similar to the $^{87}Sr/^{86}Sr$ ratios in shallow soil carbonates (e.g., BF-01), while the $^{87}Sr/^{86}Sr$ ratios in "caliche" carbonates (BF-02, 03, 04) are generally higher than those of the soil and dust carbonates in this study. For comparison, dust carbonates from El Paso pecan orchard site (Ortiz et al., 2022) have $^{87}Sr/^{86}Sr$ ratios ranging from 0.7100-0.7110 while the carbonate components in the agricultural soils have lower and narrow range of $^{87}Sr/^{86}Sr$ ratios of 0.7095-0.7100.

5. Discussion

5.1. Comparison of U-series ages of soil carbonates in natural drylands and irrigated areas

Soil carbonates from the basin floor (La Mesa) trench profile of the Jornada Basin show a wide range of U-series ages from ~719 ka to 10 ka with large ranges of uncertainties and model fits (Table 3). The long age span is generally consistent with the stable and ancient landscapes of the Jornada Basin (Gile, 2002). Indeed, the La Mesa surface at Jornada basin floor were estimated to form between middle Pleistocene (~780ka) and Late Pliocene (~1.5Ma), constrained by several studies of pumice dating and stage V soil carbonates in this area (Gile, 2002; Mack et al., 1996). The observed soil carbonate ages from this trench profile cover almost the entire landscape ages, suggesting a long and complex evolution history of the soil carbonate profile in Jornada Basin. Indeed, the dominant forms of soil carbonates observed in the trench profile are thick clast coatings, calcretes, and laminar caps (Fig. 3d). Clast coatings

form when infiltrating soil water accumulates on the lower part of rocky clasts and subsequent oversaturation of carbonates via evaporation or water uptake by roots and the timescales involved are generally on the order of thousands of years (Zamanian et al., 2016). Calcretes form when soil horizons are impregnated and cemented with soil carbonates. The high amounts of $CaCO_3$ in calcretes infer long term accumulation of Ca^{2+} and HCO_3^- on the order of tens of thousands of years or more. The sources of Ca^{2+} and HCO_3^- are generally not available locally within the soil profile and could be supplied by atmospheric deposition, unsaturated soil water flows from higher landscape positions, or fluctuating shallow groundwater table (Fig. 1c). The calcretes could significantly limit the vertical water infiltration and lead to formation of laminar caps on the top of the calcretes with timescales generally on the order of tens to hundreds of thousands of years. For comparison, a young group of soil carbonate ages (~15-120 ka by U-series dating) has been reported in two soil profiles on the Jornada I surface from the relatively younger piedmont slopes of the Jornada Basin (Table 3; Nyachoti et al., 2017). Those soil carbonates on the Jornada I surface have been characterized as carbonate nodules and clast coatings in shallow soils down to ~50cm depth and with a thin layer of calcretes commonly observed underneath (Fig. 3e), forming a low permeability boundary for infiltration of soil water. The Jornada I surface is on the piedmont slopes as a relatively younger landscape at a high topographic location, estimated to form around late to middle Pleistocene (~500-700 ka) based on stratigraphic studies (Gile, 2002).

The above conceptual models of soil carbonate formation (Zamanian et al., 2016) imply for certain stratigraphic relationships such as decreasing soil carbonate ages away from the permeability boundary (e.g., top of calcretes or bottom of rocky clasts). However, the U-series ages of the basin floor profile do not show any systematic trend with respect to their depths or relative positions on the trench (Table 3). The lack of a simple age vs. depth/distance trend is consistent with an expected complex history of such a thick soil carbonate layer that could involve precipitation, dissolution, re-precipitation, soil erosion, fractures, and overprints of layers of soil carbonates during its long period of development. Indeed, issues of soil carbonates mixed with different formation periods pose significant challenges to accurately determine their formation ages as shown by the large error bars and poorly fitting in age models in the Jornada Basin. Nevertheless, these soil carbonates still provide information with respect their environmental conditions, landscape positions, and land-use history. Indeed, soil carbonates on these two typical landscapes (basin floor and piedmont slope) in Jornada Basin formed over long-time scales (at least ~ 10ka to 100ka) in the natural Dryland CZ and once formed, these soil carbonates experienced a complex history of with features including precipitation, dissolution, and re-precipitation, potentially as a long term and stable inorganic carbon storage.

By contrast, distinctively younger soil carbonates (~2-22ka by U-series dating) have been observed in agricultural soils in El Paso, TX (Table 3; Nyachoti et al., 2017). Those soil carbonates were collected from alfalfa fields on the Rio Grande alluvial deposits and characterized as fine carbonate nodules and films and filaments (Fig. 3f), indicating very early stages of soil carbonate development. The young soil carbonates in agricultural soils highlight the possible impacts of agricultural irrigation on soil carbon dynamics in human managed dryland CZ. Indeed, Nyachoti et al. (2017) attributed these distinctively young carbonate ages from the alfalfa field to a modern addition of irrigation-induced soil carbonates due to the intensive cultivated agriculture for the last 100 years in the region. For example, the nature of the U-series ages ranging 2 - 22ka reflects a mixture of the modern soil carbonates with pre-existing old soil carbonates in the Rio Grande valley. Similarly, Ortiz et al. (2022) investigated the Sr and C isotope systematics in soil carbonates at the alfalfa field and a nearby pecan orchard and linked the Ca source to irrigation water and the C source to agricultural crops, confirming the formation of modern soil carbonates in the human managed dryland CZ. Soil carbonates formed rapidly under the impacts of irrigation in agricultural areas in the American Southwest drylands and have the potential to serve as a new inorganic carbon storage in the human-managed Dryland CZ.

5.2. Initial ($^{234}U/^{238}U$) ratios of soil carbonates recording different soil moisture conditions in dryland CZs

Initial ($^{234}U/^{238}U$) ratios recorded in the 20 natural soil carbonates on the basin floor (La Mesa surface; this study) and piedmont slope (Jornada I surface; Nyachoti et al., 2018) show a complex history of soil carbonate formation with respect to the soil moisture conditions in the Jornada Basin during the last 200 ka. The high U-series age uncertainties prevent a precise reconstruction of soil carbonate record with a detailed geochronology order. However, when considering the soil carbonates with several broadly defined age groups such as 0-15ka, 15-30ka, and 30-70ka, the initial ($^{234}U/^{238}U$) ratios show a first-order trend consistent with changes related to the glacial-interglacial periods (Table 4; Fig. 6). Indeed, initial ($^{234}U/^{238}U$) ratios of soil carbonates in Jornada Basin during the current interglacial period (0-15ka; MIS 1 or marine isotope stage 1) are mostly between 1.5 to 1.7. Consistent with this, the Rio Grande River in this region has ($^{234}U/^{234}U$) ratios of ~1.6 to 1.7, a characteristic dryland river value (Garcia et al., 2021). During most of the last glacial period (~70-30ka, e.g., MIS 5a to MIS 2), initial ($^{234}U/^{238}U$) ratios of soil carbonates are consistently lower, with values between 1.3 and 1.5 (with one exception value of 1.9). During the transition from the last glacial to interglacial period (~30-15ka), the initial ($^{234}U/^{238}U$) ratios show large variations with values increasing from ~1.0 to 1.7. Soil carbonates with ages older than ~100ka have much larger age uncertainness and initial ($^{234}U/^{238}U$) ratios between 1.1 and 1.4. Similar trends of initial ($^{234}U/^{238}U$) ratios in the last 70 ka have been observed in soil carbonates and opals in the valleys of the Great Basin and Mojave deserts in American Southwest (Maher et al., 2014). The physical locations of the Great Basin and Mojave deserts are further from our current study in southern New Mexico. However, large scale climate models have suggested that the regional climate change patterns are generally similar in American Southwest since the last ~100 ka (e.g.,Wagner et al., 2010). The observed trends of initial ($^{234}U/^{238}U$) ratios in soil carbonates in Jornada Basin in New Mexico are most likely controlled by similar soil conditions under the influence of regional climate changes in American Southwest (Oster et al., 2012; Maher et al., 2014).

Indeed, various studies have suggested that there is an intrinsic link of the ($^{234}U/^{238}U$) ratios in soil water and the availability of soil moisture that reflect regional climate parameters such as precipitation and infiltration rates, which are recorded by the initial ($^{234}U/^{238}U$) ratios in the soil carbonates at the time of carbonate formation (e.g., Maher et al., 2014). ($^{234}U/^{238}U$) ratios in soil water are sensitive to water flux due to the preferential loss of ^{234}U to the water via the energetic alpha-recoil of ^{238}U near mineral surfaces along the flow path (e.g., Chabaux et al., 2003; DePaolo et al., 2005). This theoretic framework favors the release of high ($^{234}U/^{238}U$) ratios in soil water under dry conditions with high physical weathering rates. The ($^{234}U/^{238}U$) ratios in soil water decrease with increasing amounts of precipitation and infiltration rates such as under wet conditions with high chemical weathering rates. Such an inverse relationship has been observed in about 30 global large rivers with the dissolved ($^{234}U/^{238}U$) ratios decreasing systematically with the increase of river discharges at the large watershed scale (Chabaux et al., 2008).

At the soil profile scale, soil water ($^{234}U/^{238}U$) ratios have been modelled to be inversely related to the availability of soil moisture and infiltration rates: Maher et al. (2014) has developed a simplified steady state isotope model to use the $(^{234}U/^{238}U)_0$ ratios recorded in soil minerals to constrain paleo infiltration rates:

$$q\ [mm/yr] = -16667 \ln\left(1 - \frac{F_\alpha \lambda_{234}}{10^{-2.3}(A_{sw} - A_s)}\right) \qquad \text{Eqn. 4,}$$

here q is infiltration rate (mm/yr), F_α is the alpha recoil factor of ^{238}U decay and recoil process, λ_{234} is the decay constant of ^{234}U (yr^{-1}), A_{sw} is the ($^{234}U/^{238}U$) ratio in soil water or $(^{234}U/^{238}U)_0$ ratios in soil carbonates at the time of formation, and A_s is the ($^{234}U/^{238}U$) ratio in dissolving solids (minerals in soil profile). Based on this simplified model, the $(^{234}U/^{238}U)_0$ ratios (~1.6-1.8) recorded in soil carbonates of 0-

20ka represent infiltration rates in Jornada Basin on the orders of 0.6 mm/yr in the current interglacial period (Table 4). These low values are consistent with other independent hydrological estimates in this region. For example, Walvoord and Scanlon (2004) used chloride mass balance and vadose zone flow models to show that in the New Mexico and west Texas region, vadose zone moisture and chloride depth profiles are consistent with a low recharge rate of 0.03-1.0 mm/yr in the last 15 ka, decreasing from >1.0 mm/yr in Pleistocene time (>15 ka) when the climate was wetter. Indeed, the lower $(^{234}U/^{238}U)_0$ ratios (~1.4) recorded in soil carbonates of 30-70 ka suggest a higher infiltration rate of 1.1 mm/yr, a factor of 2 increase compared to the current interglacial rates (Table 4). It is noted that the extremely low $(^{234}U/^{238}U)_0$ ratio (e.g., ~1.1) in the 20-30 ka period would suggest a high infiltration rate of ~5 mm/yr, a factor of 10 increase of the current value, during the transition from last glacial to the current inter-glacial periods (Table 4). Such a record of changing soil moisture and infiltration rates in the last 70ka at Jornada Basin is consistent with the $(^{234}U/^{238}U)_0$ records from other regions in American Southwest. For example, based on the U-series soil carbonate records from the Great Basin and Mojave deserts, the infiltration rate was generally high during 30-70ka, but a dramatic increase of infiltration rate occurred around 25ka, and the infiltration decreased significantly after the Last Glacial Maximum (LGM) (~20ka) and reached the current low infiltration rate around 15ka (Maher et al., 2014). Furthermore, a speleothem calcite record of $\delta^{18}O$ ratios (Asmerom et al., 2010) and a record of lake levels (Munroe and Laabs, 2013) from southeast New Mexico also reconstructed a precipitation history from 56ka to 11ka. The precipitation increased from ~56ka to about 25ka due to an increase of winter precipitation and decreased to current arid conditions since 15ka. These local climate records mimic the observed trends in initial $(^{234}U/^{238}U)$ ratios of Jornada soil carbonates, directly supporting the hypothesis that $(^{234}U/^{238}U)$ ratios in soil carbonates reflect availability of soil moisture and can be used as a proxy for past infiltration and precipitation.

Furthermore, soil carbonates from human impacted CZ in agricultural areas such as irrigated alfalfa fields show not only distinctively younger U-series model ages but also lower $(^{234}U/^{238}U)_0$ ratios (~1.2) when compared to natural soil carbonates from this region (Fig. 6; Nyachoti et al., 2017). The infiltration rate estimated based on the low $(^{234}U/^{238}U)_0$ ratios in the alfalfa field soil carbonates is about 1.9 mm/yr, a factor of 3-4 times higher than the rates estimated based on natural soil carbonates in this study (Table 4). The higher infiltration rate is generally consistent with the irrigation practices of local farmers who apply about ~1000 to 1500 mm/yr of Rio Grande river water or local groundwater to agricultural areas (as compared to normal rainfall at 250 mm/yr) during normal years, a factor of 4-6 time higher rate.

Alternatively, the lower $(^{234}U/^{238}U)_0$ ratios from the agricultural area soil carbonates could be contributed by low $(^{234}U/^{234}U)$ ratios from the use of phosphorus fertilizers (e.g., at 1.0). The elevated U concentrations in water from agricultural areas have been suggested as a result of the wide application of phosphorus fertilizers, which are generally enriched in U due to the co-presence of uranium and phosphorus in many phosphorous minerals. If such U in phosphorous minerals is geologically old (> 1.25 Ma), then the U released from the phosphorus fertilizers can be inferred at secular equilibrium with a characteristic $(^{234}U/^{238}U)$ ratio = 1 (Zielinski et al., 2000; Szynkiewicz et al., 2015). Indeed, the Rio Grande River in this region has $(^{234}U/^{234}U)$ ratios of ~1.6 to 1.7, a characteristic dryland river value, but the agricultural canals and drains in the Rio Grande region show significantly lower $(^{234}U/^{238}U)$ ratios (~1.1 to 1.6) that could be consistent with their interactions with fertilizer sourced U with the water flow path from agricultural fields. Hence, the lower $(^{234}U/^{238}U)_0$ ratios observed in soil carbonates from the agricultural areas in this region highlight that under human managed conditions (irrigation or fertilizer applications) new soil carbonates are actively formed and have the potential to serve as a new soil carbonate storage underneath agricultural areas in drylands and a long term C sink if the Ca ion is sourced from non-carbonate materials.

5.3. $^{87}Sr/^{86}Sr$ ratios in natural dryland carbonates and irrigated areas

Soil carbonates form under both natural and human managed dryland CZ systems and represent important inorganic carbon storages in global carbon cycles. If Ca involved in the formation of soil carbonates is from carbonate weathering such as marine carbonates or preexisting soil carbonates, the soil carbonates do not represent as a net sink of inorganic carbon storage because the carbon is derived from previous reservoirs of inorganic carbon storage (e.g., Monger et al., 2015). The long-term storage and sequestration of inorganic carbon is only valid when the Ca sources in soil carbonates are derived from silicate weathering or other non-carbonate sources (such as gypsum dissolution), as shown by numerous studies of carbon cycles, chemical weathering, and global carbon mass budget. Because of the dependence of $^{87}Sr/^{86}Sr$ ratios on lithology types, $^{87}Sr/^{86}Sr$ ratios of soil carbonates have the special power in distinguishing Ca sources, e.g., silicate vs. carbonates. The $^{87}Sr/^{86}Sr$ ratios of soil carbonates from the Jornada Basin floor site (BF01 and BF 02 at La Mesa) trench profile show a narrow range of values from 0.7085 to 0.7090 with U-series ages between 0-100 ka (Fig. 7). Such a range is close to the local rainwater or dust leachate $^{87}Sr/^{86}Sr$ ratios (e.g., soil carbonates in dust), suggesting that atmospheric wet and dry deposition have supplied the majority of Ca to the soil carbonates in Jornada Basin. The soil carbonates with these $^{87}Sr/^{86}Sr$ ratios in the last 100ka do not represent a significant long term carbon storage, as the Ca source is most likely from previously formed soil carbonates that contribute to dust or wet deposition (e.g., Capo and Chadwick, 1999). However, older soil carbonates (e.g., BF 03 and BF 04 with 100-700ka age) in this trench profile show elevated $^{87}Sr/^{86}Sr$ ratios up to 0.7100-0.7112, that could indicate different Ca sources with possible contribution of silicate weathering (Fig. 7). Indeed, silicate portions of the Jornada soils are commonly characterized by high $^{87}Sr/^{86}Sr$ ratios (Fig. 5). The elevated $^{87}Sr/^{86}Sr$ ratios indicate a possible enhanced weathering scenario under wetter climate in the past with different vegetation covers that could lead to higher soil CO_2 or root organic acids and release of Ca into soil water from silicate minerals. These group of soil carbonates with ~100-700ka ages have very large error bars of their U-series ages and hence cannot be linked to specific glacial or interglacial periods. Nonetheless, the observation of elevated $^{87}Sr/^{86}Sr$ ratios in these soil carbonates suggest the presence of a possible long term C storage and sequestration in natural drylands if Ca was released by enhanced silicate weathering in the past (Fig. 7).

Similarly, soil carbonates from agricultural areas (alfalfa and pecan farms) in this region have $^{87}Sr/^{86}Sr$ ratios of 0.7098 to 0.7102 (Fig. 7), values that are distinctive from natural rainwater, dust carbonates, or relatively younger natural soil carbonates in Jornada Basin (e.g., 0.7085-0.7090). Such a range of $^{87}Sr/^{86}Sr$ ratios is almost identical to Rio Grande river water (and local groundwater) that farmers used for irrigation in the agricultural fields (Garcia et el. 2021). The dissolved Ca from river or local groundwater have relatively high $^{87}Sr/^{86}Sr$ ratios with contribution of silicate weathering from upstream watersheds in the Rio Grande region or local alluvial aquifer systems (Garcia et al. 2021). Thus, the newly formed soil carbonates under agricultural fields in the Rio Grande valleys have potential as a long-term soil inorganic carbon storage given the involvement of Ca from non-carbonate sources.

5.4. Implications for soil inorganic carbon storage and transformation in natural and managed dryland CZ

It is generally expected that formation of soil carbonates in drylands occurred during inter-glacial periods with warm and dry climate and low soil moistures, under controls of vegetation covers (transpiration), landscape positions, and soil texture and structure. However, it is not clear if soil carbonate formation could occur under glacial periods with cooler and wetter climate especially with increased available soil water moisture, or what would happen to pre-existing soil carbonates in drylands during climate transitions from inter-glacial (warm and dry) to glacial (cool and wet) periods. With the expected increase of available soil water moisture, pre-existing soil carbonates could be dissolved, translocated to other landscape locations or aquifer, and/or re-precipitated in natural drylands. If the dissolved soil carbonate remains in groundwater aquifers underneath drylands, this process could serve as a potential short-term storage of inorganic carbon in dryland during climate transitions (e.g., Monger et

al., 2015). Such possible soil carbonate transformations highlight their important role in modulating soil inorganic carbon mass budget with repeated glacial-interglacial transitions in Earth's climate history.

In the Jornada Basin, our current studies (Table 3) quantified 20 sets of natural soil carbonate U-series ages of the basin floor (La Mesa surface) and piedmont slope (Jornada I slope), most ranging from about 200 ka to 10ka (Fig. 7). Despite the large age errors, the soil carbonates from the Jornada Basin do not show specific association with preferred formation periods either in interglacial or glacial cycles in the last 200 ka (Fig. 7). This first order observation of age patterns suggests that formation of soil carbonates in Jornada Basin possibly occurred through both the glacial and interglacial periods. Many of these soil carbonate ages, especially those older than 40ka, have large age uncertainties (> +/-30ka) and indicate a complex history of redissolution/reprecipitation and overprinting of pre-existing old soil carbonates, possibly under variable soil moisture conditions during glacial-interglacial transition periods. The long time scales involved in soil carbonate formation in natural drylands highlight their important role as a long-term sink of inorganic C. Indeed, our study of U-series and Sr isotopes highlights that ancient soil carbonates from the Jornada Basin in Chihuahuan desert contain Ca sources derived from silicate weathering in addition to carbonate sources, representing an important means of long-term carbon sequestration by natural drylands.

At the global scale, one new estimate reported that global soils store ~2305 ± 636 billon tons of inorganic carbon over the top 2-meter depth and about 1.13 ± 0.33 billon tons of inorganic carbon is lost to inland waters through soils annually, due to soil acidification associated with nitrogen additions to terrestrial ecosystems (Huang et al., 2024). Our study of initial $(^{234}U/^{238}U)_0$ and $^{87}Sr/^{86}Sr$ ratios documents that naturally occurring soil carbonates went through important transformation processes such as dissolution, reprecipitation, and translocation in response to variable soil moisture conditions caused by either long-term glacial and inter glacial transitions, or short-term modern land use changes such as agricultural practices. Soil carbonates and underlying groundwater aquifers in both natural and managed drylands could represent one important and potential missing carbon sink in the global carbonate budget (Houghton, 2007; Cole et al., 2007; Ma et al., 2014; Li et al., 2015). In addition, land use changes have greatly impacted dryland landscapes. For example, soil salinization is a common form of land degradation especially following agricultural irrigation in converted drylands (e.g., Schoups et al., 2005). Irrigated farming of the Rio Grande valley in US southwest with relatively saline water (total dissolved solids, or TDS >1000 mg/kg) from the Rio Grande and local groundwater aquifers has prevailed for the past 100 years (Ellis et al., 1993; Moore et al., 2008; Miyamoto, 2012). High concentrations of calcium and bicarbonate ions in irrigation water led to calcite saturation and precipitation in agricultural soils (Cox et al., 2018; Ortiz et al., 2022). This process affects soil quality through a reduction in soil porosity and impairment of water infiltration and plant root penetration (Entry et al., 2004; Sanderman, 2012). About two million km^2 of dryland surfaces are currently managed by irrigated agriculture, and almost 20% of irrigated drylands (~0.4 million km^2) have become salt affected, impacting soil fertility and crop growth (Ghassemi et al., 1995). At the global scale, agricultural practices in drylands alter rates of soil carbonate accumulation with great potential for carbon sequestration (e.g., Saurez, 2000; Schlesinger, 2000; Sanderman, 2012; Nyachoti et al., 2017; Ortiz et al., 2022).

6. Conclusions

U-series and Sr isotope systematics show important differences in soil carbonates formed under natural and managed dryland CZ. Soil carbonates from an ancient and stable basin floor site in the Jornada Basin in American Southwest show mature and old stage V development and U-series ages of these soil carbonates show a wide range of formation timescales from 10s ka to 100s of ka, spanning multiple glacial and interglacial stages in this region. The formation of soil carbonates is a long and

complex process, most likely independent of glacial vs. interglacial conditions. By contrast, unusually young soil carbonates are observed in agricultural areas in the Rio Grande alluvial valley with U-series ages less than 10ka, reflecting mixing and modification of natural and old soil carbonates with irrigation induced formation of soil carbonates. Indeed, initial $(^{234}U/^{238}U)_0$ activity ratios of these agricultural related soil carbonates (~1.2-1.4) are characteristically lower than those of soil carbonates from natural drylands (1.5-1.7), suggesting the changes of soil moisture conditions or additional sources of U in the agricultural area that significantly modified ($^{234}U/^{238}U$) activity ratios of soil water. Initial $(^{234}U/^{238}U)_0$ activity ratios in soil carbonates in natural drylands show systematic changes with the expected changes of soil moisture and infiltration rates from glacial and interglacial transitions. The initial $(^{234}U/^{238}U)_0$ activity ratios of soil carbonates thus show great potential to serve as indicators for soil water infiltration rates for paleoclimate studies. Furthermore, comparisons of Sr isotope ratios in soil carbonates, dust, and irrigation water allow for tracing the Ca sources in soil carbonates and evaluate their potential for long term C storage in dryland systems. Soil carbonates in both natural and managed dryland CZ can play an important role in carbon storage and transformation in global carbon budget.

Acknowledgements

We thank the field assistance from Jornada LTER. Financial support from NSF EAR 2012475 (Dryland Critical Zone network) and NSF EAR 1853680 is acknowledged.

Data Availability

Data are available through Mendeley Data at https://doi.org/10.17632/83skf8cttc.1

References:

Andersen M. B., Erel Y. and Bourdon B., 2009. Experimental evidence for ^{234}U-^{238}U fractionation during granite weathering with implications for $^{234}U/^{238}U$ in natural waters. Geochim. Cosmochim. Acta 73, 4124–4141.

Anderson S. P., von Blanckenburg F. and White A. F., 2007. Physical and chemical controls on the Critical Zone. Elements 3: 315–319.

Asmersom, Y., Polyak, V.J., and Burns, S.J. (2010), Variable winter moisture in the southwestern United States linked to rapid glacial climate shifts. Nature Geoscience, 3, 114-117. Doi: 10.1038/NGEO754.

Bataille, C., and Bowen, G., 2012. Mapping $^{87}Sr/^{86}Sr$ variations in bedrock and water for large scale provenance studies. Chemical Geology 304-305, 39-52.

Bergametti, G. and Gillette, D. A., 2010. Aeolian sediment fluxes measured over various plant/soil complexes in the Chihuahuan desert. Journal of Geophysical Research 115, F03044, 10.1029/2009JF001543.

Birkeland, P.W., 1999. Soils and Geomorphology. Oxford University Press, New York, 430 pp.

Bischoff, J.L. and Fitzpatrick, J.A., 1991. U-Series Dating of Impure Carbonates - an Isochron Technique Using Total-Sample Dissolution. Geochimica Et Cosmochimica Acta 55, 543-554.

Bourdon, B., Turner, S., Henderson, G. M., Lundstrom, C. C., 2003. Introduction to U-series geochemistry. Reviews in Mineralogy and Geochemistry 52, 1-21.

Brantley, S. L., White, T. S., White, A. F., Sparks, D., Richter, D., Prgitzer, K., Derry, L., Chorover, J., Chadwick, O., April, R., Anderson, S. and Amundson, R., 2006. Frontiers in exploration of the Critical Zone: Report of a workshop sponsored by the National Science Foundation (NSF), October 24–26, 2005, Newark, DE. p. 30.

Brantley, S.L., J.P. Megonigal, F.N. Scatena, Z. Balogh-Brunstad, R.T. Barnes, M.A. Bruns, P. van Cappelen, K. Dontsova, H. Hartnett, T. Hartshorn, A. Heimsath, E. Herndon, Jin, L., C.K. Keller, J.R. Leake, W.H. McDowell, F.C. Meinzer, T. Mozder, S. Petsch, J. Pett-Ridge, P. Raymond, C.S. Riebe, K. Shumaker, A. Sutton-Grier, R. Walter, and K. Yoo., 2011. Twelve testable hypotheses on the geobiology of weathering. Geobiology 9, 140-165.

Brooks, P. D., Chorover, J., Fan, Y., Godsey, S. E., Maxwell, R. M., McNamara, J. P., and Tague, C., 2015. Hydrological partitioning in the critical zone: Recent advances and opportunities for developing transferable understanding of water cycle dynamics. Water Resources Research 51, 6973–6987.

Buck, B. J. and Monger, H. C.,1999. Stable isotopes and soil- geomorphology as indicators of Holocene climate change, northern Chihuahuan Desert. Journal of Arid Environments 43, 357–373.

Bullen, T.D., Krabbenhoft, D.P., Kendall, C., 1996. Kinetic and mineralogic controls on the evolution of groundwater chemistry and $^{87}Sr/^{86}Sr$ in a sandy silicate aquifer, northern Wisconsin, USA. Geochemica et Cosmohimca Acta 60,1807-1821.

Candy, I., 2002. Formation of a rhizogenic calcrete during a glacial stage (Oxygen Isotope Stage 12): its palaeoenvironmental and stratigraphic significance. Proceedings of the Geologists' Association, 113, 259 – 270.

Capo, R. C. and Chadwick, O. A., 1999. Sources of strontium and calcium in desert soil and calcrete. Earth and Planetary Science Letters 170, 61-72.

Capo, R. C., Stewart, B. W., Chadwick, O. A., 1998. Strontium isotopes as tracers of ecosystem processes: theory and methods. Geoderma 82, 197-225.

Cerling, T. E., 1984. The stable isotopic composition of modern soil carbonate and its relationship to climate. Earth Planetary Science Letters 71, 229–240.

Chabaux, F., Bourdon, B., and Riotte, J., 2008. U-series geochemistry in weathering profiles, river waters and lakes. Radioactivity in the Environment 13, 49-104.

Chabaux, F., Riotte, J., Dequincey, O., 2003. U-Th-Ra fractionation during weathering and river transport. Reviews in Mineralogy and Geochemistry 52, 533-576.

Chadwick, O.A., Derry, L.A., Vitousek, P.M., Huebert, B.J., Hedin, L.O., 1999. Changing sources of nutrients during four million years of ecosystem development. Nature 397 (6719), 491–497.

Cheng, H., Edwards, R. L., Hoff, J., Gallup, C. D., Richards, D. A., Asmerom, Y., 2000. The half-lives of uranium-234 and thorium-230. Chemical Geology, 169(1), 17-33.

Chiquet, A., Michard, A., Nahon, D., Hamelin, B., 1999. Atmospheric input vs in situ weathering in the genesis of calcretes: an Sr isotope study at Gálvez (Central Spain). Geochimica et Cosmochimica Acta 63(3), 311-323.

Clark, K.I., Fritz P., 1997. Environmental Isotopes in Hydrogeology. Lewis Publishers, New York, pp. 328.

Cole, J. J., Prairie, Y. T., Caraco, N. F., McDowell, W. H., Tranvik, L. J., Striegl, R. G., Duarte, C. M., Kortelainen, P., Downing, J. A., Middelburg, J. J., and Melack, J., 2007. Plumbing the global carbon cycle: Integrating inland waters into the terrestrial carbon budget, Ecosystems 10, 171–184.

Cox, C., L. Jin, G. Ganjegunte, D. Borrok, V. Lougheed, and L. Ma., 2018. Soil quality changes due to flood irrigation in agricultural fields along the Rio Grande in western Texas. Applied Geochemistry 90, 87-100.

DePaolo, D.J., Maher, K., Christensen, J.N., McManus, J., 2006. Sediment transport time measured with U-series isotopes: results from ODP North Atlantic drift site 984. Earth Planet. Sci. Lett. 248, 394–410.

Deutz, P., Montanez, I.P., Monger, C.H. 2002. Morphology and Stable and Radiogenic Isotope Composition of Pedogenic Carbonates in Late Quaternary Relict Soils, New Mexico, U.S.A.: An Integrated Record of Pedogenic Overprinting. Journal of Sedimentary Research 72(6), 809-822.

Driese, S.G. and Mora, C.K. 1993. Physico-chemical environment of pedogenic carbonate formation in Devonian vertic paleosols, central Appalachians, USA. Sedimentology 40, 199–216.

Duffy, C., Shi, Y, Davis, K., Slingerland, R., Li, L., Sullivan, P.L., Goddéris, Y. and Brantley, S.L., 2014. Designing a suite of models to explore Critical Zone function. Procedia Earth and Planetary Science 10, 7-15.

Duniway, M.C., Petrie, M.D., Peters, D.C, Anderson JP, Crossland K, Herrick JE 2018. Soil water dynamics at 15 locations distributed across a desert landscape: insights from a 27-yr dataset. Ecosphere 9(7), 36pp.

Duniway, M.C., Snyder, K.A., Herrick, J.E. , 2010. Spatial and temporal patterns of water availability in a grass-shrub ecotone and implications for grassland recovery in arid environments. Ecohydrology. 3, 55-67.

Durand, N., Gunnell, Y., Curmi, P., Ahmad, S. M., 2007. Pedogenic carbonates on Precambrian silicate rocks in South India: Origin and paleoclimatic significance. Quaternary International, 162, 35-49.

Edwards, R.L., Gallup, C.D. and Cheng, H., 2003. Uranium-series Dating of Marine and Lacustrine Carbonates. Reviews in Mineralogy and Geochemistry 52, 363-405.

Egli, M., and Fitze, P., 2001. Quantitative aspects of carbonate leaching of soils with differing ages and climates. Catena 46, 35-62.

Ellis, S. R., Levings, G. W., Carter, L. F., Richey, S. F. and Radell, M. J. 1993. Rio Grande valley, Colorado, New Mexico, and Texas. Journal of the American Water Resources Association 29, 617–646.

Entry, J. A., Sojka, R. E. & Shewmaker, G. E., 2004. Irrigation increases inorganic carbon in agricultural soils. Environ. Manag. 33(S1), S309–S317.

Eswaran, H., Reich, P.F., Kimble, J.M., Beinroth, F.H., Padmanabhan, E., Moncharoen, P., 2000. Global carbon stocks. In: Lal, R., Kimble, J.M., Eswaran, H., Stewart, B.A. (Eds.), Global Climate Change and Pedogenic Carbonates. Lewis Publishers, Boca Raton, FL, 15-25.

Feng, S. and Fu, Q., 2013. Expansion of global drylands under warming climate. Atmospheric Chemistry and Physics 13(19), 10.5194/acp-13-10081-2013.

Fleischer, R. L., 1980. Isotopic Disequilibrium of Uranium: Alpha-Recoil Damage and Preferential Solution Effects. Science, 207, 979.

Gaillardet, J., I. Braud, F. Hankard, S. Anquetin, O. Bour, N. Dorfliger, et al. 2018. OZCAR: The French network of critical zone observatories. Vadose Zone J. 17, 180067, 10.2136/vzj2018.04.0067.

Garcia S, Louvat P, Gaillardet J, Nyachoti S, and Ma, L., 2021. Combining Uranium, Boron, and Strontium Isotope Ratios ($^{234}U/^{238}U$, $\delta^{11}B$, $^{87}Sr/^{86}Sr$) to Trace and Quantify Salinity Contributions to Rio Grande River in Southwestern United States. Front. Water 2, 575216. 10.3389/frwa.2020.575216.

Gibbens, R. P., McNeely, R. P., Havstad, K. M., Beck, R. F., Nolen, B., 2005. Vegetation changes in the Jornada Basin from 1858 to 1998. Journal of Arid Environments 61, 651– 668.

Ghassemi, F., Jakeman, A. J. & Nix, H. A., 1995. Salinisation of Land and Water Resources: Human Causes, Extent, Management and Case Studies 526, CABI Publishing.

Gile, L. H., 2002. Lake Jornada, an early-middle Pleistocene lake in the Jornada del Muerto Basin, southern New Mexico. New Mexico Geology, 24(1), 3-14.

Gile, L.H., Hawley, J.W., Grossman, R.B., 1981. Soils and geomorphology in the Basin and Range area of Southern New Mexico: Guidebook to the Desert Project. New Mexico Bureau of Mines and Mineral Resources., Socorro, NM, 222 pp.

Gillette, D. A., 1999. A qualitative geophysical explanation for hot spot dust emitting source regions. Contributions to Atmospheric Physics 72(1), 67-77.

Gillette, D. A. and Chen, W., 2001. Particle production and aeolian transport from a “supply-limited” source area in the Chihuahuan desert, New Mexico, United States. Journal of Geophysical Research: Atmospheres 106(D6), 5267-5278.

Grace, J., José, J. S., Meir, P., Miranda, H. S., & Montes, R. A., 2006. Productivity and carbon fluxes of tropical savannas. Journal of Bioge-ography, 33(3), 387–400.

Hawley, J. W., 1981. Pleistocene and Pliocene history of the international boundary area, southern New Mexico. Hoffer, J-. M., Hoffer, RL (eds.), Geology of the border, 26-32.

Hirmas, D.R., Amrhein, C., Graham, R.C., 2010. Spatial and process-based modeling of soil inorganic carbon storage in an arid piedmont. Geoderma 154: 486-494.

Houghton, R. A., 2007. Balancing the global carbon budget. Annu. Rev. Earth Pl. Sc., 35, 313–347.

Jafari, H., Raeisi, E., Hoehn, E., Zare, M., 2012. Hydrochemical characteristics of irrigation return flow in semi-arid regions of Iran. Hydrol. Sci. J. 57, 173–185.

Jochum, K.P., Weis, U., Schwager, B., Stoll, B., Wilson, S.A., Haug, G.H., Andreae, M.O. and Enzweiler, J., 2016. Reference values following ISO guidelines for frequently requested rock reference materials. Geostandards and Geoanalytical Research, 40(3), 333-350.

Klose, M., Gill, T. E., Etyemezian, V., Nikolich, G., Zadeh, Z. G., Webb, N. P., and Van Pelt, R. S., 2019. Dust emission from crusted surfaces: Insights from field measurements and modelling. Aeolian Research, 40, 1-14.

Konter, J.G., Storm, L.P., 2014. High precision $^{87}Sr/^{86}Sr$ measurements by MC-ICP-MS, simultaneously solving for Kr interferences and mass-based fractionation, Chemical Geology, 385, 26-34.

Lal, R. and Kimble, J.M., 2000. Pedogenic carbonates and the global carbon cycle. In: R. Lal, J.M. Kimble, H. Eswaran and B.A. Stewart (Editors), Global climate change and pedogenic carbonates. Lewis Publishers, Boca Raton, 1-14.

Laudicina, V.A., Scalenghe, R., Piscoiotta, A., Parello, F., Dazzi, C., 2013. Pedogenic carbonates and carbon pools in gypsiferous soils of a semiarid Mediterranean environment in south Italy. Geoderma 192: 31-38.

Li, Y., Wang, Y. G., Houghton, R. A., and Tang, L. S., 2015. Hidden carbon sink beneath desert, Geophys. Res. Lett., 42, 5880–5887.

Ludwig, K.R., 2003. Mathematical-statistical treatment of data and errors for $^{230}Th/U$ geochronology. Uranium- Series Geochemistry, Reviews in Minerology and Geochemistry, 52: 631-656.

Luo, S., and Ku, T. L., 1991. U-series isochron dating: A generalized method employing total-sample dissolution. Geochimica et Cosmochimica Acta 55, 555–564.

Ma, J., Liu, R., Tang, L.-S., Lan, Z.-D., and Li, Y., 2014. A downward CO_2 flux seems to have nowhere to go. Biogeosciences, 11, 6251–6262.

Mack, G. H., Giordano, T. H., Cole, D. R., James, W. C., Salyards, S. L., 1994. Stable oxygen and carbon isotopes of pedogenic carbonate as indicators of Plio-Pleistocene paleoclimate in the southern Rio Grande Rift, south-central New Mexico. American Journal of Science 294(5), 621-640.

Mack, G.H., Salyards, S.L., James, W.C., 1993. Magnetostratigraphy of the Plio-Pleistocene Camp Rice and Palomas Formations in the Rio Grande rift of southern New Mexico. American Journal of Science 293, 49-77.

Mack, G. H., McIntosh, W. C., Leeder, M. R., Monger, H. C., 1996. Plio-Pleistocene pumice floods in the ancestral Rio Grande, southern Rio Grande rift, USA. Sedimentary Geology 103(1), 1-8.

Mack, G. H., Salyards, S. L., McIntosh, W. C., Leeder, M. R., 1998. Reversal magnetostratigraphy and radioisotopic geochronology of the Plio-Pleistocene Camp Rice and Palomas Formations, southern Rio Grande rift. Guidebook 49, 229-236.

Mack, G. H., Jones, M. C., Tabor, N. J., Ramos, F. C., Scott, S. R., Witcher, J. C., 2012. Mixed Geothermal and Shallow Meteoric Origin of Opal and Calcite Beds In Pliocene–Lower Pleistocene Axial–Fluvial Strata, Southern Rio Grande Rift, Rincon Hills, New Mexico, USA. Journal of Sedimentary Research 82(8), 616-631.

Maher, K., C. I. Steefel, D. J. DePaolo, and B. E. Viani., 2006. The mineral dissolution rate conundrum: Insights from reactive transport modelling of U isotopes and pore fluid chemistry in marine sediments. Geochimica et Cosmochimica Acta, 70, 337–363.

Maher, K., DePaolo, D.J., Lin, J.C.F., 2004. Rates of silicate dissolution in deep-sea sediment: In situ measurement using $^{234}U/^{238}U$ of pore fluids. Geochim. Cosmochim. Acta 68 (22), 4629–4648.

Maher, K., Ibarra, D.E., Oster, J.L., Miller, D.M., Redwine, J.L., Reheis, M.C., Harden, J.W., 2014. Uranium isotopes in soils as a proxy for past infiltration and precipitation across the western United States. Am. J. Sci. 314, 821–857.

Menozzi, D., Dosseto, A. & Kinsley, L. P. J., 2016. Assessing the effect of sequential extraction on the uranium-series isotopic composition of a basaltic weathering profile. Chemical Geology, 446 126-137.

McGee, D., Quade, J., Edward, R.L., Broecker, W.S., Cheng, H., Reiners, P.W., Evenson, N., 2012. Lacustrine cave carbonates: Novel archives of paleohydrologic change in the Bonneville Basin (Utah, USA). Earth Planet. Sci. Lett. 351-352, 182–194.

Miyamoto, S., 2012. Salinization of Irrigated Urban Soils: A Case Study of El Paso, Texas. Texas A&M University, Texas Water Resources Institute, TR-433.

Monger, H.C. and Martinez-Rios, J.J., 2001. Inorganic carbon sequestration in grazing lands. In R. F. Follett, J. M. Kimble, & R. Lal (Eds.), The potential of U.S. grazing lands to sequester carbon and mitigate the greenhouse effect, 87–118. Boca Raton, FL: Lewis Publishers.

Monger, H.C., 2003. Millennial-scale climate variability and ecosystem response at the Jornada LTER site. In: Greenland, D., Goodin, D.G., Smith, R.C. (Eds.), Climate Variability and Ecosystem Response at Long-Term Ecological Research Sites. Oxford University Press, London, 341–369.

Monger, H.C., 2006. Regional Setting of the Jornada Basin. In: Havstad, K., Huenneke, l.F., Schlesinger, W.H. (Eds.), Structure and Function of Chihuahuan desert Ecosystem: The Jornada Basin Long-Term Ecological Research Site. Oxford University Press, pp. 492.

Monger, H.C., Cole, D.R., Buck, B.J., Gallegos, R.A., 2009. Scale and the isotopic record of C4 plants in pedogenic carbonate: from the biome to the rhizosphere. Ecology 90 (6), 1498-1511.

Monger, H.C., Kraimer, R.A., Khresat, S., Cole, D.R., Wang, W. and Wang, J., 2015. Sequestration of inorganic carbon in soil and groundwater. Geology 43 (5), 375-378.

Moore, S.J., Bassett, R.L., Liu, B., Wolf, C.P., Doremus, D. 2008. Geochemical tracers to evaluate hydrogeologic controls on river salinization, Groundwater, 46, 489-501.

Munroe, J.S., and Laabs, B.J.C. (2013), Temporal correspondence between pluvial lake highstands in the southwestern US and Heinrich Event 1. Journal of Quaternary Science, 28, 49-58. doi: 10.1002/jqs.2586.

Naiman, Z., Quade, J., & Patchett, P. J., 2000. Isotopic evidence for eolian recycling of pedogenic carbonate and variations in carbonate dust sources throughout the southwest United States. Geochimica et Cosmochimica Acta,64(18), 3099-3109.

Newman, B. D., Wilcox, B. P., Archer, S. R., Breshears, D. D., Dahm, C. N., Duffy, C. J., 2006. Ecohydrology of water-limited environments: A scientific vision. Water Resources Research, 42, W06302.

Neymark, L.A., 2011, Potential effects of alpha-recoil on uranium-series dating of calcrete. Chemical Geology, 282(3-4): 98-112.

Nicholson, S. E., 2011. Dryland climatology. Cambridge, UK: Cambridge University Press.

Nordt, L., Orosz, M., Driese, S., Tubbs, J., 2006. Vertisol carbonate properties in relation to mean annual precipitation: implications for paleoprecipitation estimates. The Journal of geology, 114(4), 501-510.

Noy-Meir, I., 1973. Desert ecosystems: Environment and producers. Annual Review of Ecology and Systematics, 4(1), 25–51.

Nyachoti, S., Jin, L., Tweedie, C.E., Ma, L., 2017. Formation of pedogenic carbonates in the semi-arid Rio Grande valley: insights from carbon, major elements, and U-series isotopes in natural and agricultural soils of southern New Mexico and western Texas. Chemical Geology, 10.1016/j.chemgeo.2017.10.014.

Ortiz, A.C., Jin, L., Ogrinc, N. et al., 2022. Dryland irrigation increases accumulation rates of pedogenic carbonate and releases soil abiotic CO_2. Sci Rep 12, 464.

Osmond, J.K., May, J.P., and Tanner, W.F., 1970. Age of the Cap Kennedy barrier-and-lagoon complex. J. Geophys. Res. 75, 5459-5468.

Oster, J.L., Montañez, I.P., Kelley, N.P., 2012. Response of a modern cave system to large seasonal precipitation variability. Geochim. Cosmochim. Acta 91, 92-108.

Oster, J, Kitajima, K., Valley, J. Rogers, B., and Maher, K., 2017. An evaluation of paired $\delta^{18}O$ and $(^{234}U/^{238}U)_0$ in opal as a tool for paleoclimate reconstruction in semi-arid environments. Chemical Geology 449, 236-252.

Paces, J.B., and Whelan, J.F., 2012. The paleohydrology of unsaturated and saturated zones at Yucca Mountain, Nevada, and vicinity, in Stuckless, J.S., ed., Hydrology and Geochemistry of Yucca Mountain and Vicinity, Southern Nevada and California: Geological Society of America Memoir 209, 219-276.

Pelt, E., Chabaux, F., Innocent, C., Navarre-Sitchler, A. K., Sak, P. B., Brantley, S. L., 2008. Uranium–thorium chronometry of weathering rinds: rock alteration rate and paleo-isotopic record of weathering fluids. Earth and Planetary Science Letters 276(1), 98-105.

Pett-Ridge, Julie C., Louis A. Derry, and Andrew C. Kurtz., 2009. Sr isotopes as a tracer of weathering processes and dust inputs in a tropical granitoid watershed, Luquillo Mountains, Puerto Rico. Geochimica et Cosmochimica Acta 73, 25-43.

Pravalie, R., 2016. Drylands extent and environmental issues. A global approach. Earth-Science Reviews 161, 259–278.

Rasmussen C, Pelletier JD, Troch PA, Swetnam TL and Chorover J, 2015. Quantifying topographic and vegetation effects on the transfer of energy and mass to the Critical Zone. Vadose Zone Journal 14(11), 10.2136/vzj2014.07.0102.

Rath, K. and Rousk, J., 2015. Salt effects on the soil microbial decomposer community and their role in organic carbon cycling: a review. Soil Biology and Biochemistry 81, 108-123.

Retallack, G.J., 1994. The environmental factor approach to the interpretation of palaeosols. In: Amundson, R., Harden, J., Singer, M. (Eds), Factors of Soil Formation: A Fiftieth Anniversary Retrospective. Soil Science Society of America, Madison, Wisconsin, 31–64.

Retallack, G.J., 2005. Pedogenic carbonate proxies for amount and seasonality of precipitation in paleosols. Geology 33, 333–336.

Reynolds, J. F., Kemp, P. R., Ogle, K., & Fernández, R. J., 2004. Modifying the 'pulse-reserve' paradigm for deserts of North America: Precipitation pulses, soil water, and plant responses. Oecologia, 141(2), 194–210.

Rivera, N. I. R., Gill, T. E., Bleiweiss, M. P., & Hand, J. L., 2010. Source characteristics of hazardous Chihuahuan Desert dust outbreaks. Atmospheric environment 44(20), 2457-2468.

Robinson, L.F., Henderson, G.M., Hall, L., Matthews, I., 2004. Climatic control of riverine and seawater uranium-isotope ratios. Science 305, 851–854.

Rosholt, J.N., 1976, $^{230}Th/^{234}U$ dating of travertine and caliche rinds, GSA Prog. 8, 1076.

Royer, D.L., 1999. Depth to pedogenic carbonate horizon as a paleoprecipitation indicator?: Geology 27, 1123-1126.

Sanderman, J, 2012. Can management induced changes in the carbonate system drive soil carbon sequestration? A review with particular focus on Australia. Agriculture, Ecosystems & Environment 155, 70-77.

Schlesinger, W. H., 2000. Carbon sequestration in soils: Some cautions amidst optimism. Agric. Ecosyst. Environ. 82, 121–127.

Schlesinger, W.H., 1982. Carbon storage in the caliche of arid soils: a case study from Arizona. Soil Science 133, 247-255.

Schoups, G., Hopmans, J.W., Young, C.A., Vrugt, J.A., Wanllender, W.W. and Tanji, K.K., 2005. Sustainability of irrigated agriculture in the San Joaquin Valley, California. PNAS 102 (43), 15352-15356.

Scott, R. L., and Biederman, J. A., 2019. Critical zone water balance over 13 years in a semiarid savanna. Water Resources Research, 55, 574–588.

Seager, W. R., Shafiqullah, M., Hawley, J. W., & Marvin, R., 1984. New K-Ar dates from basalts and the evolution of the southern Rio Grande rift. Geological Society of America Bulletin 95(1), 87-99.

Serna-Perez, A., Monger, H.C., Herrick, J.E., and Murray, L., 2006. Carbon dioxide emissions from exhumed petrocalcic horizons. Soil Science Society of America Journal 70, 795–805.

Sheta, A.S., Al-Sewailem, M.S., Sallam, A. Sh., Al-Mashhady, A.S., 2000. Nature and composition of newly formed precipitates in relationship to characteristics of groundwater in arid environment. Arid Soil Res. Rehabil. 14, 387–401.

Sims, K.W.W., J.B. Gill, A. Dosseto, D.L. Hoffmann, C.C. Lundstrom, R.W. Williams, L. Ball, D. Tollstrup, S. Turner, J. Prytulak, J.J.G. Glessner, J.J. Standish, and T. Elliott, 2008. An Inter-Laboratory Assessment of the Thorium Isotopic Composition of Synthetic and Rock Reference Materials. Geostandards and Geoanalytical Research, 32 (1), 65-91.

Smith, D.B., Solano, Federico, Woodruff, L.G., Cannon, W.F., and Ellefsen, K.J., 2019. Geochemical and mineralogical maps, with interpretation, for soils of the conterminous United States: U.S. Geological Survey Scientific Investigations Report 2017-5118,

Snyder, K. A. and Tartowski, S. L., 2006. Multi-scale temporal variation in water availability: implications for vegetation dynamics in arid and semi-arid ecosystems. Journal of Arid Environments 65(2), 219-234.

Sobecki, T. M., and Wilding, L. M., 1983. Formation of calcic and argillic horizons in selected soils of the Texas coast prairie. Soil science society of America Journal 47, 707-715.

Strandmann, P.A.E. Pogge von K.W. Burton, R.H. James, P. van Calsteren, S.R. Gislason, 2010. Assessing the role of climate on uranium and lithium isotope behaviour in rivers draining a basaltic terrain. Chem. Geol. 270, 227-239.

Suarez, D. L., 2000. Impact of agriculture on CO2 as affected by changes in inorganic carbon'. In Global Climate Change and Pedogenic Carbonates (eds Lal, R. et al.), 257–272, CRC/Lewis Publishers.

Sullivan PL, Ma L, West N, Jin L, Karwan DL, Noireaux J, Steinhoefel G, Gaines KP, Eissenstat DM, Gaillardet J, Derry LA, Meek K, Hynek S, and Brantley SL, 2016. CZ-tope at Susquehanna Shale Hills CZO:Synthesizing multiple isotope proxies to elucidate Critical Zone processes across timescales in a temperate forested landscape. Chemical Geology, 445, pp.103-119.

Sullivan, P.L., Goddéris, Y., Shi, Y., Gu, X., Schott, J., Hasenmueller, E. A., Kaye, J., Duffy, C., Jin, L., and Brantley, S. L., 2019. Exploring the effect of aspect to inform future earthcasts of climate driven changes in weathering of Shale. Journal of Geophysical Research: Earth Surface, 124, 974–993.

Szynkiewicz, A., Borrok, D.M., Ganjegunte, G.K., Skrzypek, G., Ma, L., Rearick, M.S., Perkins, G.B. 2015. Isotopic studies of the Upper and Middle Rio Grande. Part 2- Salt loads and human impacts in south New Mexico and west Texas, Chemical Geology 411, 336-350.

Tabor, N.J., Montanez, I.P., Kelso, K.A., Currie, B.S., Shippman, T.A., 2006. A late Triassic soil catena: landscape controls on paleosol morphology across the Carnian–Age Ischigualasto–Villa Union Basin, Northwestern Argentina. In: Alonso-Zarza, A.M., Tanner, L.H. (Eds.), Paleoenvironmental Record and Applications of Calcretes and Palustrine Carbonates. Geological Society of America Special Paper, 416, 17–41.

Tanner, L., 2010. Continental carbonates as indicators of paleoclimate. Developments in sedimentology, 62, 181 – 188.

Tripathy, G.R., Singh S. K., Krishnaswami, S., 2010. Sr and Nd isotopes as tracers of chemical and physical Erosion. In Handbooks of Environmental Isotope Geochemistry, edited by Baskaran, M., pp 521-552.

United Nations Convention to Combat Desertification (UNCCD), 2000. Fact Sheet 2: The Causes of Desertification. United Nations Secretariat of the Convention to Combat Desertification.

Van Devender, T.R., 1990. Late Quaternary vegetation and climate of the Chihuahuan desert, United States and Mexico. In: Betancourt, J.L., Van Devender, T.R., Martin, P.S. (Eds.), Packrat Middens - the Last 40,000 Years of Biotic Change. University of Arizona Press, Tucson, pp. 104-133.

Van Devender, T.R., 1995. Desert grassland history: changing climates, evolution, biogeography and community dynamics. In: McClaran, M.P., Van Devender, T.R. (Eds.), The Desert Grassland. University of Arizona Press, Tucson, AZ, USA, 68–99.

Vermeesch, P., 2018. IsoplotR: a free and open toolbox for geochronology. Geoscience Frontiers 9, 1479-1493.

Violette, A., Riotte, J., Braun, J., Oliva, P., Marechal, J., Sekhar, M., Jeandel, C., Subramanian, S., Prunier, J., Barbiero, L. and Dupre, B., 2010. Formation and preservation of pedogenic carbonates in Southern Indian, links with paleo-monsoon and pedological conditions: Clues from Sr isotopes, U-Th series and REEs. Geochimica et Cosmochimica Acta 74, 7059-7085.

Wagner, J.D.M., Cole, J.E., Beck, J.W., Patchett, P.J., Henderson, G.M., and Barnett, H.R. (2010), Moisture variability in the southwestern United States linked to abrupt glacial climate change. Nature Geoscience, 3, 110-113. Doi:10.1038/NGEO707.

Wang, L., D'Odorico, P., Evans, J. P., Eldridge, D. J., McCabe, M. F., Caylor, K. K., 2012. Dryland ecohydrology and climate change: Critical issues and technical advances. Hydrology Earth Syst. Sci. 16 (8), 2585–2603.

Weems, S. L. and Monger, H. C., 2012. Banded vegetation-dune development during the Medieval Warm Period and 20th century, Chihuahuan Desert, New Mexico, USA. Ecosphere 3(3), 21.

Walvoord, M. and Scanlon, B. R., 2004. Hydrologic processes in deep vadose zones in inter-drainage arid environments. Groundwater Recharge in a Desert Environment: The Southwestern United States. Editors: Hogan, F., Phillips, F.M., Scanlon, B.R., 10.1029/009WAS02.

White T, Brantley SL, Banwart S, Chorover J, Dietrich W, Derry L, Lohse K, Anderson S, Aufdendkampe A, Bales R, Kumar P, Richter D, and McDowell B, 2015. The role of critical zone observatories in critical zone science, in Principles and Dynamics of the Critical Zone, (eds. R. Giardino and C. Hauser), Elsevier. Chapter 2, Developments in Earth Surface Processes 19, 15–78.

Wymore AS, West N, Maher K, Sullivan PL, Harpold A, Karwan DL, Marshall JA, Perdrial J, Rempe D, and Ma L, 2017. Growing new generations of critical zone scientists. Earth Surface Processes and Landforms. doi:10.1002/esp.4196

Zamanian, K., Pustovoytov, K. and Kuzyakov, Y., 2016. Pedogenic carbonates: Forms and formation processes. Earth-Science Reviews 157, 1–17.

Zielinski, R. A., K. R. Simmons, and W. H. Orem., 2000. Use of ^{234}U and ^{238}U isotopes to identify fertilizer-derived uranium in the Florida Everglades. Applied Geochemistry 15, 369–383.

Figure captions

Figure 1. a) A general map of Chihuahuan Desert in American Southwest drylands and the study area in southern New Mexico and west Texas; **b)** a general soil profile of carbonate formation and accumulation. The soil profile is consistent of soil A, B, and C horizon. Soil carbonates generally accumulate at the bottom of the B layer and in the C layer. Rainfall (P) and evapotranspiration **(**ET) control soil moisture availability and water infiltration flux (P-ET). The depth scale is approximately ~2m. **c)** Soil carbonate formation and evolution: forms and stages (I: needle, fiber, powder, II: nodule, coating, III: calcrete, IV and V: laminar caps; Gile, 1981) of soil carbonates vary with time, landscape position, soil texture, and soil water flows and groundwater flows (blue arrows; modified after Zamanian et al., 2016). The depth scale is approximately ~2m.

Figure 2. A block diagram of the Jornada Basin and nearby Rio Grande alluvial valley in the Chihuahuan Desert, modified after Monger et al. (2006). Approximate locations of the Basin floor (BF) site and the piedmont slope (PD) site in Jornada Basin and the agricultural sites (AG) in the Rio Grande alluvial valley are indicated. Study areas are part of the U. S. National Science Foundation Critical Zone Collaborative Network (CZCN) and the Jornada Basin is also part of the Long Term Ecological Research (LTER) Network.

Figure 3. Representative soil profiles and site photos for the basin floor site (A), piedmont slope site (B), and agricultural site (C). Forms and features of soil carbonates from each site are shown at various scales. Laminar cap at the basin floor site (D), thick clast coating from the piedmont site (E) and fine needles and fiber (F) at the alfalfa agricultural sites under optical microscope.

Figure 4. A) ($^{234}U/^{238}U$) activity ratios of Jornada Basin Floor soil carbonate samples (BF-series) from the La Mesa trench profile. Bulk soil carbonate samples are shown in brown circles. Weak acid leachate (1M HCl or 1M acetic acid) samples are shown in blue squares, representing carbonate portion of bulk samples. Leachate residue samples are shown in red diamonds, representing silicate portion of bulk samples. Bulk dust samples are shown in light green circles. Red dashed line indicates U-series secular equilibrium (1.0) and blue dashed line represents average ($^{234}U/^{238}U$) ratios (~1.7) in Rio Grande river water (Garcia et al., 2021).

B) ($^{234}U/^{238}U$) and ($^{230}Th/^{238}U$) activity ratios of Jornada Basin Floor soil carbonate samples (BF-series in brown circles) from the La Mesa trench profile, Jornada Piedmont Slope (PD-series in blue squares) and nearby agricultural sites (AG-series in green triangles). BF-. PD-, and AG-series samples are all weak acid leachate samples, presenting carbonate portion of bulk samples. Background grids show evolution of ($^{234}U/^{238}U$) and ($^{230}Th/^{238}U$) activity ratios as a function initial $(^{234}U/^{238}U)_0$ ratios (from 0.8 to 2.0, with incremental change of 0.1) and carbonate ages (from 0 ka to 500 ka, with incremental change of 10ka). Four BF samples (BF01, BF 07, BF 08, and BF09) were plotted out of the U-series evolution curves.

Figure 5. $^{87}Sr/^{86}Sr$ ratios of Jornada Basin Floor soil carbonate samples (BF-series) from the La Mesa trench profile. Weak acid leachate (1M HCl or 1M acetic acid) samples are shown in blue squares, representing carbonate portion of bulk samples. Leachate residue samples are shown in red diamonds, representing silicate portion of bulk samples. Jornada dust samples are shown at 0 cm depth. Light blue box indicates the range of $^{87}Sr/^{86}Sr$ ratios from rain and modern carbonate dust in this region (Capo and Chadwick, 1999).

Figure 6. Initial $(^{234}U/^{238}U)_0$ ratios vs. U-series model ages calculated for Jornada Basin Floor soil carbonates (BF-series in brown circles) of the La Mesa trench profile, Jornada Piedmont slope soil carbonates (PD-series in blue squares), and Rio Grande alluvial valley agricultural soil carbonates (AG-series in green diamonds). PD and AG samples were reported in Nyachoti et al. (2017). Large blue circle indicates ($^{234}U/^{238}U$) ratios of Rio Grande river water (~1.7; Garcia et al., 2021). Marine Isotope Stages (MIS) and glacial/interglacial stages are indicated. Thick grey line represents the long term trend of the data points, analyzed by Matlab function, trenddecomp (). Numbered dashed black lines indicate characteristic initial $(^{234}U/^{238}U)_0$ ratios for interglacial period (~1.4 for ~70ka to 30ka), transition period into the last glacial period (~1.05 at ~30ka to 20ka), current interglacial period (~1.7 at 20ka to present), and modified soil carbonates on agricultural sites (~1.2; Table 4).

Figure 7. $^{87}Sr/^{86}Sr$ ratios of soil carbonates, extracted by using weak acid leachates, in Jornada Basin Floor soil carbonate samples (BF-series) from the La Mesa trench profile vs. their U-series model ages. Blue boxes indicate the ranges of soil carbonates with ages <100ka vs. >100ka. Light blue squares indicate dust carbonates analyzed in this study. Green box indicates the range soil carbonates from agricultural sites (55 soil samples from pecan fields and alfalfa sites; from Ortiz et al., 2022). Dashed blue box indicates the range of Rio Grande water (source of irrigation water; Garcia et al., 2021; Ortiz et al., 2022).

Table 1. U-series concentrations and activity ratios for soil carbonates from Jornada Basin.

Sample ID	Field ID	Profile Depth (cm)	Analytical Method	Sub Sample ID	Uranium Content (mg/Kg)	+/- (2σ)	Thorium Content (mg/Kg)	+/- (2σ)	($^{230}Th/^{232}Th$)	+/- (2σ)	($^{230}Th/^{238}U$)	+/- (2σ)	($^{234}U/^{238}U$)	+/- (2σ)	($^{232}Th/^{238}U$)	+/- (2σ)
BF 01	H1	40	LR	Bulk	1.59	0.02	6.02	0.06	0.620	0.006	0.770	0.012	0.911	0.005	1.242	0.015
				HCl R	0.96	0.01	4.23	0.04	0.917	0.009	1.327	0.021	0.915	0.005	1.447	0.017
				AcOH R	0.68	0.01	4.30	0.04	0.886	0.009	1.825	0.029	0.913	0.005	2.059	0.025
				HCl L	0.04	0.00	0.17	0.00	0.897	0.009	1.192	0.019	1.098	0.005	1.328	0.016
				AcOH L	0.06	0.00	0.28	0.00	0.840	0.008	1.426	0.023	0.997	0.005	1.697	0.020
BF 02	H2A	60	LR	Bulk	0.99	0.01	2.55	0.03	0.887	0.009	0.747	0.012	1.192	0.006	0.843	0.010
				HCl R	0.72	0.01	2.84	0.03	0.734	0.007	0.949	0.015	1.005	0.005	1.292	0.016
				AcOH R	0.69	0.01	2.05	0.02	0.945	0.009	0.916	0.015	1.015	0.005	0.970	0.012
				HCl L	0.39	0.00	0.41	0.00	1.411	0.014	0.484	0.008	1.483	0.007	0.343	0.004

			AcOH L	0.35	0.00	0.34	0.00	1.473	0.015	0.470	0.008	1.500	0.007	0.319	0.004
	H2B	60	TD	Bulk	1.13	0.01	2.45	0.02	0.976	0.010	0.697	0.011	1.211	0.006	0.714	0.009
				Bulk	1.17	0.01	2.41	0.02	0.984	0.010	0.666	0.011	1.262	0.006	0.677	0.008
				Bulk	1.24	0.01	1.80	0.02	1.392	0.014	0.660	0.011	1.304	0.007	0.474	0.006
	H2C	60	LR	Bulk	1.42	0.01	1.85	0.02	1.188	0.012	0.506	0.008	1.365	0.007	0.426	0.005
				HCl R	0.49	0.01	1.39	0.01	0.953	0.010	0.889	0.014	1.120	0.006	0.932	0.011
				AcOH R	0.73	0.01	1.69	0.02	1.223	0.012	0.926	0.015	1.133	0.006	0.758	0.009
				HCl L	0.90	0.01	0.36	0.00	2.080	0.021	0.273	0.004	1.516	0.008	0.131	0.002
				AcOH L	0.35	0.00	0.29	0.00	2.050	0.020	0.231	0.004	1.515	0.008	0.113	0.001
			TD	Bulk	1.34	0.01	1.94	0.02	1.103	0.011	0.524	0.008	1.340	0.007	0.475	0.006
				Bulk	1.45	0.01	2.04	0.02	1.072	0.011	0.492	0.008	1.355	0.007	0.459	0.006
				Bulk	1.64	0.01	2.03	0.02	1.290	0.013	0.521	0.008	1.341	0.007	0.404	0.005
BF	03	H3A	200	LR	Bulk	2.07	0.02	2.39	0.02	2.636	0.026	0.999	0.016	1.016	0.005	0.379	0.005
					HCl R	1.03	0.01	1.71	0.02	1.679	0.017	0.914	0.015	0.955	0.005	0.544	0.007
					AcOH R	1.20	0.01	1.83	0.02	1.917	0.019	0.956	0.015	0.987	0.005	0.499	0.006

			HCl L	0.92	0.01	0.81	0.01	3.826	0.038	1.096	0.018	1.080	0.005	0.287	0.003
			AcOH L	0.83	0.01	0.57	0.01	4.838	0.048	1.088	0.017	1.080	0.005	0.225	0.003
	H3C	200	LR	Bulk	1.67	0.02	2.86	0.02	1.738	0.017	0.978	0.016	0.980	0.005	0.562	0.007
				HCl R	0.88	0.01	1.65	0.02	1.447	0.014	0.882	0.014	0.884	0.004	0.610	0.007
				AcOH R	0.91	0.01	1.86	0.02	1.348	0.013	0.900	0.014	0.883	0.004	0.668	0.008
				HCl L	0.77	0.01	1.07	0.02	2.480	0.025	1.122	0.018	1.094	0.005	0.452	0.005
				AcOH L	1.15	0.01	0.81	0.02	3.014	0.030	0.689	0.011	1.097	0.005	0.229	0.003
			TD	Bulk	3.66	0.04	2.84	0.03	3.917	0.039	0.991	0.016	1.079	0.005	0.253	0.003
				Bulk	2.24	0.02	2.12	0.02	3.242	0.032	1.005	0.016	1.034	0.005	0.310	0.004
				Bulk	2.04	0.02	2.51	0.03	2.525	0.025	1.015	0.016	1.043	0.005	0.402	0.005
BF 04	H4B	60	TD	Bulk	0.60	0.01	0.95	0.01	1.960	0.020	1.021	0.016	1.147	0.006	0.521	0.006
				Bulk	0.50	0.01	1.17	0.01	1.286	0.013	0.986	0.016	1.259	0.006	0.767	0.009
				Bulk	0.62	0.01	1.12	0.01	1.769	0.018	1.051	0.017	1.144	0.006	0.594	0.007
	H4C	60	TD	Bulk	0.46	0.01	1.21	0.01	1.128	0.011	0.967	0.015	1.186	0.006	0.857	0.010
				Bulk	0.55	0.01	1.57	0.02	1.016	0.010	0.958	0.015	1.177	0.006	0.943	0.011

				Bulk	0.48	0.01	1.68	0.02	0.836	0.008	0.962	0.015	1.112	0.006	1.151	0.014
BF 05	J1	60	TD	Bulk	0.74	0.01	0.59	0.01	3.288	0.033	0.863	0.009	1.359	0.007	0.262	0.003
BF 06	J2	100	LR	Bulk	1.01	0.01	1.39	0.01	1.912	0.019	0.859	0.009	1.339	0.007	0.449	0.005
				AcOH L	0.73	0.01	0.87	0.01	2.025	0.020	0.785	0.008	1.362	0.007	0.388	0.005
				AcOH R	0.35	0.00	0.68	0.01	1.804	0.018	1.158	0.012	1.228	0.006	0.642	0.008
BF 07	J3	140	LR	Bulk	0.81	0.01	0.92	0.01	4.202	0.042	1.562	0.016	1.262	0.006	0.372	0.004
				AcOH L	0.23	0.00	0.23	0.00	5.807	0.058	1.904	0.019	1.319	0.007	0.328	0.004
				AcOH R	0.62	0.01	0.83	0.01	3.184	0.032	1.393	0.014	1.255	0.006	0.438	0.005
BF 08	J5	200	LR	Bulk	3.36	0.03	1.34	0.01	9.896	0.099	1.296	0.013	1.083	0.005	0.131	0.002
				AcOH L	0.89	0.01	0.28	0.00	10.832	0.108	1.124	0.011	1.128	0.006	0.104	0.001
				AcOH R	2.60	0.03	0.93	0.01	11.513	0.115	1.347	0.013	1.068	0.005	0.117	0.001
BF 09	J6	170	LR	Bulk	2.72	0.03	2.30	0.02	3.573	0.036	0.988	0.010	0.929	0.005	0.276	0.003
				AcOH L	0.44	0.00	0.46	0.00	3.329	0.033	1.150	0.011	0.935	0.005	0.345	0.004
				AcOH R	2.35	0.02	2.46	0.02	2.715	0.027	0.932	0.009	0.933	0.005	0.343	0.004

TD: total digestion; LR: leaching and residue pairs;

Weak leachates include 1M HCl and 1M acetate acid (AcOH).

Sample Name	Sample type	$^{87}Sr/^{86}Sr$	+/-	$^{87}Sr/^{86}Sr$	+/-	$^{87}Sr/^{86}Sr$	+/-
		Weak acid leachate (L)		Residue (R)		Bulk	
M-Rabb	Dust	0.7087	0.0001	0.7165	0.0001		
M-well	Dust	0.7091	0.0001	0.7225	0.0001		
G-IBPE4	Dust	0.7087	0.0001	0.7190	0.0001		
P-Tobo	Dust	0.7088	0.0001	0.7147	0.0001		
P-Coli	Dust	0.7086	0.0001	0.7119	0.0001		
T-TYL	Dust	0.7087	0.0001	0.7190	0.0001	0.7184	0.0001
T-East	Dust	0.7088	0.0001	0.7134	0.0001	0.7141	0.0001
M-Rabb	Dust	0.7088	0.0001	0.7151	0.0001		
M-well	Dust	0.7090	0.0001	0.7164	0.0001		
G-IBPE4	Dust	0.7088	0.0001	0.7220	0.0001		
P-Tobo	Dust	0.7088	0.0001	0.7150	0.0001		
P-Coli	Dust	0.7087	0.0001	0.7119	0.0001		
T-TYL	Dust	0.7088	0.0001	0.7158	0.0001	0.7170	0.0001
T-East	Dust	0.7089	0.0001	0.7127	0.0001	0.7126	0.0001
H1	Soil arbonate	0.7086	0.0001	0.7250	0.0001	0.7230	0.0001
H2C	Soil carbonate	0.7089	0.0001	0.7140	0.0001	0.7101	0.0001

Table 2.

H2B	Soil carbonate	0.7090	0.0001	0.7190	0.0001	0.7123	0.0001
H2A	Soil carbonate	0.7089	0.0001	0.7200	0.0001	0.7120	0.0001
H3C	Soil carbonate	0.7111	0.0001	0.7140	0.0001	0.7115	0.0001
H3B	Soil carbonate	0.7112	0.0001	0.7160	0.0001	0.7115	0.0001
H3A	Soil carbonate	0.7112	0.0001	0.7140	0.0001	0.7114	0.0001
H4C	Soil carbonate	0.7091	0.0001	0.7098	0.0001	0.7098	0.0001
H4B	Soil carbonate	0.7101	0.0001	0.7104	0.0001	0.7104	0.0001
H4A	Soil carbonate	0.7102	0.0001	0.7200	0.0001	0.7107	0.0001

$^{87}Sr/^{86}Sr$ ratios of dust and soil carbonate from Jornada Basin

Sample Name	Sub Sample ID	Method	Model	U-series ages (ka)	Uncer. (+)	Uncer. (-)	$(^{234}U/^{238}U)_0$	Uncer. (+/-)	MSWD	P (chi 2)	N
BF 02	H2A	L_R	R_M1	21	1.4	9.5	1.68	0.01	29	0.00	5
BF 02	H2B	TD	R_M1	56	9	62.9	1.47	0.047	10	0.00	3
BF 02	H2C	L_R + TD	R_M1	10	0.57	2.36	1.58	0.011	14	0.00	8
BF 03	H3A	L_R	R_M1	455	228	570	1.18	0.015	4	0.00	5
BF 03	H3C	L_R + TD	R_M1	111	6.89	72.56	1.223	0.011	90	0.00	8
BF 04	H4B	TD	R_M1	719	NaN	NaN	0.868	0.048	10	0.00	3
BF 04	H4C	TD	R_M1	117	28.8	28.8	1.417	0.058	1.2	0.29	3
BF 06	J2	TD	R_M1	15	4.9	4.9	1.58	0.037	0.88	0.42	3
BF 08	J5	TD	R_M1	24	9.4	214	1.32	0.037	110	0.00	3
BF 05	J1	TD	Single Age	66	0.2	0.2	1.43				1
Piedmont Sites											
JPTI 0-10cm				44	32	32	1.89	0.51			
JPTI 10-15cm				17.1	6	6	1.5	0.09			
JPTI 15-20cm				30	11	11	1.46	0.09			

JPTI 25-30cm	14.5	6.8	6.8	1.64	0.13
JPTI 40cm	117	26	26	1.4	0.11
JPTII 0-7cm	68	110	110	1.38	0.09
JPTII 7-10cm	29	13	13	1.03	0.06
JPTII 27-30cm	19.5	7.5	7.5	1.5	0.08
JPTII 37-40cm	50	21	21	1.4	0.07
JPTII 48cm	100	40	40	1.32	0.08
Agricultural Sites					
AG 0-3cm	15	17	17	1.49	0.06
AG 10-13cm	6.5	8.7	8.7	1.52	0.08
AG 20-23cm	9.1	8.6	8.6	1.59	0.11
AG 30-33cm	5.1	5.7	5.7	1.32	0.14
AG 40-43cm	2.2	1.7	1.7	1.47	0.06
AG 50-53cm	2.9	1.9	1.9	1.25	0.09
AG 60-63cm	22.2	8.1	8.1	1.23	0.24

Table 3. U-series ages and initial (234U/238)0 ratios of soil carbonate estimated with Isoplot R.

Note: U-series ages and initial $(^{234}U/^{238}U)_0$ ratios of soil carbonates from the basin floor trench profile were calculated with the program ISOPLOT R (Ludwig, 2003; Vermeesch, 2018). The sets of cogenetic samples were generally obtained from using several sub-samples (total sample digestion or TD method)

or combining acid leachate/residual samples (L-R method). The isochron fitting model is R_M1, the Rosholt Maximum likelihood model. MSWD is mean square of weighted deviates and p (chi2) is probability of fit. N represents the numbers of samples on each isochron. U-series ages and initial $(^{234}U/^{238}U)_0$ ratios of soil carbonates for Piedmont slope and agricultural sites were reported in Nyachoti et al. (2017).

Scenario	q[a] (mm/yr)	f α	$\lambda^{234}U$ (yr^{-1})	Asw	As	Notes[b]
1. Last glacial stage *(30-70ka)*	1.1 ± 0.2	0.05	2.83×10^{-6}	1.4 ± 0.2	0.95	A moderate increase (~30%) of precipitation recorded for America Southwest (Maher et al., 2014)
2. Last Transition stage *(20-30ka)*	4.7 ± 0.9	0.05	2.83×10^{-6}	1.05 ± 0.2	0.95	An enhanced precipitation increased (~100%) recorded for America Southwest ((Maher et al., 2014)
3. Current Interglacial *(0-20ka)*	0.6 ± 0.1	0.05	2.83×10^{-6}	1.7 ± 0.1	0.95	Deep vadose zone flux on the order of 0.01-0.1 mm/yr (Walvoord and Scanlon, 2004)
4. Modern agricultural areas in dryland	1.9 ± 0.2	0.05	2.83×10^{-6}	1.2 ± 0.1	0.95	Irrigation in this area used equivalent of 500-1250 mm/yr water compared to nautral precipitation ~250 mm/yr (e.g., Ortiz et al., 2022)

Table 4. Estimated soil water infiltration rates based on $(^{234}U/^{238}U)_0$ initial ratios recorded by soil carbonates in this study

a. q, soil water infiltration rate (mm/yr), was estimated based on the conceptual model (equation 4) by Maher et al. (2014). $\lambda^{234}U$ is the decay constant (yr^{-1}) for ^{234}U. Asw is characteristic soil water ($^{234}U/^{238}U$) ratios, estimated based on soil carbonate records in this study and Nyachoti et al. (2019) and Ortiz et al. (2022), Rio Grande river water, and

agricultural drain water (Garcia et al., 2021) for each scenario. As is ($^{234}U/^{238}U$) ratios in dissolving minerals in soils, estimated based on soil U isotope ratios in this region from Syprose et al. (2017). $f\alpha$ is the alpha recoil factor, assuming to be 0.05 for a steady state recoil process in dissolving soil minerals with As = 0.95, $f\alpha$ = 1-As; the $f\alpha$ is also consistent with typical literature values (Maher et al., 2006).

b. Independent studies and references to support the estimated soil water infiltration rates.